

Integral Line-of-Sight Guidance and Control of Underactuated Marine Vehicles: Theory, Simulations and Experiments

Walter Caharija, Kristin Y. Pettersen, Marco Bibuli, Pedro Calado, Enrica Zereik, José Braga, Jan T. Gravdahl, Asgeir J. Sørensen, Milan Milovanović, Gabriele Bruzzone

Abstract—This paper presents an extensive analysis of the integral line-of-sight (ILOS) guidance method for path following tasks of underactuated marine vehicles, operating on and below the sea surface. It is shown that due to the embedded integral action, the guidance law makes the vessels follow straight lines by compensating for the drift effect of environmental disturbances such as currents, wind and waves. The ILOS guidance is first applied to a 2D model of surface vessels that includes the underactuated sway dynamics of the vehicle as well as disturbances in the form of constant irrotational ocean currents and constant dynamic, attitude dependent, forces. The actuated dynamics are not taken into account at this point. A Lyapunov closed loop analysis yields explicit bounds on the guidance law gains to guarantee uniform global asymptotic stability (UGAS) and uniform local exponential stability (ULES).

The complete kinematic and dynamic closed loop system of the 3D ILOS guidance law is analyzed next, hence extending the analysis to underactuated AUVs for 3D straight-line path following applications in the presence of constant irrotational ocean currents. The actuated surge, pitch and yaw dynamics are included in the analysis where the closed loop system forms a cascade, and the properties of UGAS and ULES are shown. The 3D ILOS control system is a generalization of the 2D ILOS guidance. Finally, results from simulations and experiments are presented to validate and illustrate the theoretical results, where the 2D ILOS guidance is applied to the CART and the LAUV vehicles.

Index Terms—Path following, LOS guidance, Nonlinear control, Underactuated vessels, Experiments, CART USSV, LAUV

I. INTRODUCTION

Environmental forces and disturbances such as ocean currents, wind and waves are often referred to as sea loads [1], and their effect can significantly undermine maritime activities and pose serious threats to the people involved. The unavoidable occurrence of dealing with heavy seas and the need to guarantee ship maneuverability as well as safety of the crew on board has lead to improved vessel hulls, smarter navigation techniques and better meteorological forecasts.

Unmanned marine vehicles such as autonomous underwater vehicles (AUVs), remotely operated vehicles (ROVs) and unmanned surface vehicles (USV) make it possible to operate in otherwise hazardous and inaccessible areas for humans (deep waters or under the ice). In particular, AUVs are becoming more popular and are starting to replace ROVs in activities such as search and rescue, surveying and pipeline inspection [2]. The unmanned USVs are also experiencing a significant development phase: [3] demonstrates that cooperating USVs can perform emergency towing operations, while in [4] a USV is used to retrieve overboard personnel.

Supported by the Research Council of Norway through the Centres of Excellence funding scheme, project number 223254 and the Strategic University Program, project number 192427.

W. Caharija, K. Y. Pettersen and A. J. Sørensen are with the Centre for Autonomous Marine Operations and Systems, NTNU, Trondheim, Norway. {walter.caharija,kristin.y.pettersen}@itk.ntnu.no, asgeir.sorensen@ntnu.no

J. T. Gravdahl is with the Dept. of Engineering Cybernetics, NTNU, Trondheim, Norway. jan.tommy.gravdahl@itk.ntnu.no

M. Bibuli, E. Zereik and G. Bruzzone are with ISSIA-CNR, Genova, Italy. {marco.bibuli,enrica.zereik,gabriele.bruzzone}@ge.issia.cnr.it

P. Calado and J. Braga are with LSTS, University of Porto, Portugal. {pdcalado,jose.braga}@fe.up.pt

M. Milovanović is with Rolls-Royce Marine AS, Bergen, Norway. milan.milovanovic@rolls-royce.com

Most marine surface vessels are underactuated since they are equipped with fixed stern propellers and steering rudders, or alternatively with azimuth thrusters only. Even when tunnel thrusters are installed, such actuators are effective exclusively at low maneuvering speeds [5]. Similar arguments apply to underwater vehicles: most existing AUVs are torpedo shaped and equipped with stern propellers, steering rudders and diving rudders only [6]. As a result, the absence of actuation in sway/heave poses significant challenges on the control system design side in path following and trajectory tracking scenarios, especially when the vessel is subject to disturbances acting in the underactuated transverse directions.

Whether on the surface or under the surface, many offshore oil and gas activities involve path following tasks of marine vessels. Path following is a motion control scenario where a vessel or underwater vehicle has to follow a predefined path without any time constraints. For a detailed discussion on the fundamental differences between different motion control scenarios the reader is referred to [7]–[10]. A review of different approaches to path following and other control problems of marine vehicles and vessels is given in [11], [12] where both linear and nonlinear control strategies are used. In particular, nonlinear control approaches have become popular since they take into account the dominating nonlinear behavior, and reduced-state stabilization techniques are often used to address nonlinear control problems involving underactuated marine vessels. For instance, [13] proposes a nonlinear controller for 2D path following tasks of 3 degrees-of-freedom (DOFs) underactuated marine vehicles. The work of [13] is further developed in [14] and [15], where 3D and 2D path following is considered.

Stabilizing all the DOFs of an underactuated vehicle using a single controller is an ambitious and powerful approach since it gives complete control over the vehicle. The work of [16] presents one of the first solutions to the full-state stabilization problem of underactuated 3-DOFs surface vessels. In [16], the controllers are designed to make the vessel follow a 2D path and to stabilize the heading dynamics. These results are improved in [17] and extended to trajectory tracking in [18]. Motivated by [16], [19] presents a path following control solution for a 3-DOFs underactuated marine vehicle required to follow a straight line. These results are extended to underactuated underwater vehicles for path following of 3D curves in [20]. The Lyapunov direct method and backstepping techniques are exploited for full-state stabilization of underactuated 3-DOFs surface vessels for tracking and path following scenarios in [21], [22].

This paper focuses on the nonlinear line-of-sight (LOS) guidance principle. The nonlinear LOS law is widely used to solve practical path following problems of marine vehicles due to its simplicity and intuitiveness: it imitates a helmsman steering the vessel toward a point lying at a constant distance ahead of the ship along the desired path. In particular, it is used in [23]–[27] for path following control in 2D of fully actuated as well as underactuated ships. In [25] the LOS guidance law for 3-DOFs underactuated surface vessels is tested on a model ship but the zero dynamics and the cross-track error dynamics are not analyzed. The work of [25] is further developed in [28], [29]. The complete kinematic/dynamic closed loop behavior of a LOS guidance system is analyzed in detail with a full state approach

in [26] where explicit stability conditions upon the guidance law parameters are given. The preliminary results of [26] are validated with experiments in [30]. The LOS guidance is used in [31] for 3D path following control of underactuated underwater vehicles where a full-state stabilization approach is followed to show stability. To render the LOS guidance robust with respect to disturbances such as ocean currents, [32] proposes a modification based on measurements of the AUV velocity, while [33] suggests to directly control the relative velocity of the vehicle and to estimate the necessary crab angle. Both the contributions refer to planar motion. Planar motion is also considered in [34], [35] where integral action is added to the LOS reference generator to compensate for ocean currents without the need for velocity measurements or disturbance estimators. In [35] the possibility of spatial and temporal integral effects is mentioned, while [34] shows convergence with an extensive mathematical full-state stabilization approach since absolute velocities as well as relative velocities are present in the system dynamics, forcing the introduction of adaptive techniques, and thus increasing complexity and weakening stability. Course control, integral action and adaptive techniques are added to the LOS in [36], [37] and a reduced-state stabilization approach is followed without however analyzing the underactuated sway dynamics of the ship. Semiglobal stability properties of LOS guidance systems are argued in [38]. The Integral Line-of-Sight (ILOS) guidance first proposed in [34] is analyzed with full-state stabilization and a relative velocity approach in [39] for surface vessels (2D) and in [40] for underwater vehicles (3D). In both cases global κ -exponential stability is shown. The results of [39] are integrated with intuitive arguments and a robustness analysis in [41].

This paper aims to improve, extend and validate the ILOS guidance law presented in [39]–[42] and its contributions are as follows: first a general theoretical framework is established where both kinematic as well as dynamic disturbances are taken into account to show that the ILOS guidance law can handle environmental loads of different nature and to therefore generalize the partial results given in [39]–[42]. In this context currents and wind forces are considered, given their significance. These results are then applied to underactuated AUVs and, compared to [40], the stability analysis is improved giving more precise bounds. Finally, compared to [39]–[42], an extensive set of simulations and field experiments on the CART surface vehicle and the LAUV vehicle are presented to validate and illustrate the ILOS guidance concept. The paper is hence organized in three main parts: the first (Section II) introducing the general theoretical framework, the second (Section III) applying the results to underactuated AUVs and the third (Section IV) showing the simulation and the experiments. Each part has its own introduction.

Finally, notice that in this paper the crab angle is defined as the difference between the heading of the vessel and its course. In the 3D case there is hence two crab angles: the yaw crab angle in the horizontal plane and the pitch crab angle in the vertical plane. This is consistent with the definition of crab angle used in aeronautics [43].

II. THE UNDERACTUATED DYNAMICS IN ILOS GUIDANCE SCHEMES

Planar motion is considered in this part of the paper and the ILOS guidance is shown to be robust with respect to both kinematic as well as dynamic disturbances in the underactuated sway direction. A simplified model that includes the underactuated sway dynamics is used to derive explicit bounds for the choice of the ILOS guidance gains (the look ahead distance and the integral gain). Although the model does not take into account the actuated surge and yaw dynamics, the Lyapunov analysis is more complete than similar kinematic or reduced-state stabilization approaches presented in [36]–[38], [44]. Both kinematic as well as dynamic disturbances are

taken into account to show that the ILOS guidance law can handle environmental loads of different nature. In particular, currents and wind forces are considered in this context, given their significance [45]–[47]. The strong stability results of uniform global asymptotic stability (UGAS) and uniform local exponential stability (ULES), or equivalently global κ -exponential stability [48], are shown for path following of straight lines.

The presentation is organized as follows: in Section II-A the model of the vessel that includes the sway dynamics is presented, in Section II-B the integral LOS guidance law is introduced and in Section II-C the stability properties of the closed loop system are given. The stability analysis is given in Section II-D. Finally, conclusions are given in Section II-E.

A. The Model of the Vessel and the Control Objective

In this section the model of the vessel that includes the sway dynamics is presented and the control objective is defined. The actuated surge and yaw dynamics are not taken into account.

1) *The Model of the Vessel:* The following simplified model is used to describe the motion of the vessel in this part of the paper:

$$\dot{x} = \cos(\psi_d)u_{rd} - \sin(\psi_d)v_r + V_x, \quad (1a)$$

$$\dot{y} = \sin(\psi_d)u_{rd} + \cos(\psi_d)v_r + V_y, \quad (1b)$$

$$\dot{v}_r = X(u_{rd})\dot{\psi}_d + Y(u_{rd})v_r + w_v, \quad (1c)$$

where x and y describe the position of the vessel in the inertial frame, and v_r is its relative sway velocity. The terms u_{rd} and ψ_d represent the desired surge relative velocity and heading angle set by the speed and heading controllers, respectively. The detailed surge and yaw dynamics are not considered and hence u_{rd} and ψ_d are the control inputs of (1). The functions $X(u_r)$ and $Y(u_r)$ satisfy the following assumptions:

Assumption II.1. The functions $X(u_r)$ and $Y(u_r)$ are continuous and bounded for bounded arguments.

Assumption II.2. $Y(u_r)$ is such that $|Y(u_r)|$ is strictly increasing for $u_r > 0$ and satisfies $Y(u_r) \leq -Y^{\min} < 0$, $\forall u_r \in [-V_{\max}, U_{rd}]$, where Y^{\min} is a positive constant.

The constant current components in the inertial frame, V_x and V_y , represent the kinematic disturbance. Notice that V_x and V_y are bounded, i.e. there exists a $V_{\max} > 0$ such that $V_{\max} \geq \sqrt{V_x^2 + V_y^2}$. The term w_v is a bias term that embodies unmodeled dynamics and dynamic, heading dependent, disturbances caused by currents, winds and waves. In this part of the paper, the effects of constant wind disturbances acting in a constant direction $\beta_e \in [0, 2\pi]$ are considered in w_v . Hence, the term w_v is:

$$w_v \triangleq \kappa_v(\gamma_e) \sin(\beta_e - \psi), \quad (2)$$

where $\gamma_e = \psi - \beta_e - \pi$ is the angle of attack of the wind, and the function $\kappa_v(\gamma_e)$ satisfies the following assumptions:

Assumption II.3. The function κ_v is bounded, periodic of class C^1 with bounded first derivative. Therefore, there exists $\kappa_v^{\max}, \kappa_v^{\prime \max}$ such that $\kappa_v(\cdot) \leq \kappa_v^{\max}$, $\frac{d\kappa_v(\cdot)}{d\cdot} \leq \kappa_v^{\prime \max}$.

Assumption II.4. The function κ_v is such that, given any constants $k \in \mathbb{R}$ and $\beta_e \in [0, 2\pi]$, the following bound holds for all $s \in \mathbb{R}$:

$$\left| \kappa_v(\gamma_e^k) - \kappa_v(\gamma_e^{k+s}) \frac{\sqrt{k^2 + 1}}{\sqrt{(s+k)^2 + 1}} \right| \leq \kappa_v^{\max} \frac{|s|}{\sqrt{(s+k)^2 + 1}}, \quad (3)$$

where $\gamma_e^k \triangleq -\tan^{-1}(k) - \beta_e - \pi$ and $\gamma_e^{k+s} \triangleq -\tan^{-1}(k+s) - \beta_e - \pi$.

Remark II.1. Notice that the wind load coefficients given in [45], [46], [49] can be shown to satisfy Assumptions II.3-II.4, or can be easily approximated with functions satisfying Assumptions II.3-II.4.

Remark II.2. Notice that there is no control input in (1c) that can directly compensate for the sway drift nor for the dynamic disturbance w_v .

Remark II.3. A detailed description of the derivation of (1) is here omitted since it is covered by Section III.

2) *The Control Objective:* The control system should make the vessel follow a given straight line \mathcal{P} . This should also hold in the presence of disturbances modeled as a combination of a constant and irrotational ocean current and a dynamic heading dependent force acting in the underactuated sway direction. To simplify the problem without any loss of generality since coordinates can always be rotated given a desired direction in the plane, the inertial reference frame i is placed such that the x -axis is aligned with the desired path $\mathcal{P} \triangleq \{(x, y) \in \mathbb{R}^2 : y = 0\}$. The y coordinate then corresponds to the cross-track error and the goals the control system should pursue are formalized as follows:

$$\lim_{t \rightarrow \infty} y(t) = 0, \quad (4)$$

$$\lim_{t \rightarrow \infty} \psi_d(t) = \psi_{ss}, \quad \psi_{ss} \in \left(-\frac{\pi}{2}, \frac{\pi}{2}\right), \quad (5)$$

where ψ_{ss} is constant. Notice that $\psi(t)$ is not required to converge to zero but rather to a steady-state constant value bounded within $-\frac{\pi}{2}$ and $\frac{\pi}{2}$. In particular, the ship is required to hold a non-zero yaw angle at equilibrium. This is necessary because the vessel is underactuated and no control forces are available in sway to counteract the drift forces acting in this direction. The value of ψ_{ss} will be specified later.

The relative velocity needs to be sufficiently large to guarantee ship maneuverability in presence of disturbances. In particular, it is shown in this paper that the following assumption guarantees path following in presence of kinematic and dynamic disturbances acting in any direction:

Assumption II.5. The desired constant relative surge velocity is given by $u_{rd} \triangleq U_{rd}$ and satisfies the following condition:

$$U_{rd} > \max \left\{ V_{\max} + \frac{5}{2} \left| \frac{\kappa_v^{\max}}{Y(U_{rd})} \right|, 2V_{\max} + 2 \left| \frac{\kappa_v^{\max} + \kappa_v'^{\max}}{Y(U_{rd})} \right| \right\},$$

Remark II.4. It is always possible to find values of U_{rd} satisfying Assumption II.5, since $|Y(u_r)|$ is strictly increasing for $u_r > 0$.

B. The Integral Line of Sight Guidance Law

The ILOS guidance law first developed in [34] is presented in this section. The surface vessel has to converge and follow the x -axis despite the presence of environmental disturbances. The desired heading angle is defined by the following ILOS guidance law:

$$\psi_{\text{ILOS}} \triangleq -\tan^{-1} \left(\frac{y + \sigma y_{\text{int}}}{\Delta} \right), \quad \Delta, \sigma > 0, \quad (6a)$$

$$\dot{y}_{\text{int}} = \frac{\Delta y}{(y + \sigma y_{\text{int}})^2 + \Delta^2}. \quad (6b)$$

The constant design parameters Δ and σ are the look-ahead distance and the integral gain, respectively. The integral effect becomes significant when disturbances push the craft away from its path. This gives a nonzero angle (6a) and makes the vessel crab while staying on the desired path, so that part of its relative forward velocity can counteract the effect of the environmental disturbances, as shown in Fig. 1. Notice that the law (6b) reduces the risk of wind-up since it gives less integral action when the vehicle is far from \mathcal{P} .

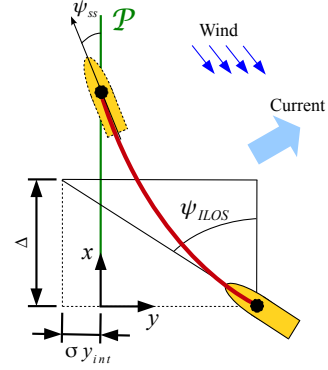


Fig. 1. Integral line of sight guidance for an underactuated surface vessel. At steady state the nonzero angle ψ_{ss} allows the underactuated vehicle to counteract the disturbances.

C. Stability Conditions

This section presents the main result of this part, including the stability conditions under which the proposed ILOS guidance (6) achieves the objectives (4-5). The notation $X^{U_{rd}} \triangleq X(U_{rd})$ and $Y^{U_{rd}} \triangleq Y(U_{rd})$ is used.

Theorem II.1. *Given an underactuated surface vessel described by the dynamical system (1). If Assumptions II.1-II.5 hold and, if the look-ahead distance Δ and the integral gain σ satisfy the conditions:*

$$\Delta > \frac{|X^{U_{rd}}|}{|Y^{U_{rd}}|} \Omega(\sigma) \left[\frac{5}{4} \frac{U_{rd} + V_{\max} + \sigma}{U_{rd} - V_{\max} - \sigma} + 1 \right], \quad (7)$$

$$0 < \sigma < U_{rd} - V_{\max} - \frac{5}{2} \left| \frac{\kappa_v^{\max}}{Y^{U_{rd}}} \right|, \quad (8)$$

where $\Omega(\sigma)$ is defined as,

$$\Omega(\sigma) \triangleq \frac{U_{rd} - V_{\max} - \sigma}{U_{rd} - V_{\max} - \sigma - \frac{5}{2} \left| \frac{\kappa_v^{\max}}{Y^{U_{rd}}} \right|}, \quad (9)$$

then $u_{rd} \triangleq U_{rd}$ and $\psi_{rd} = \psi_{\text{ILOS}}$ given by (6) guarantee achievement of the control objectives (4-5).

Remark II.5. The lower bound (7) is expected and has a clear physical interpretation: a too short look-ahead distance $\Delta > 0$ makes the vessel overshoot the target and thus causes chattering [44]. Moreover, notice that the yaw rate $\dot{\psi}_d$ in (1c) acts as a perturbation of the sway dynamics. In particular, if the sway motion is only lightly damped, i.e. if $X^{U_{rd}} \gg Y^{U_{rd}}$, then the yaw rate has a significant influence on the sway relative velocity v_r . Hence, the yaw rate must be limited to make sure that the sway dynamics behave properly. This is done by increasing the look-ahead distance Δ as suggested by the lower bound (7). A larger Δ makes the vessel turn slower, thus smoothing and limiting its yaw rate. The overall effect is a virtual increase in damping in sway. In the opposite case, when $X^{U_{rd}} \ll Y^{U_{rd}}$, damping is higher and hence the vessel can tolerate a higher yaw rate. In this case a shorter Δ can be used and the vessel is capable of more aggressive maneuvers. This confirms the analysis from [44], [50] where it is argued that longer look-ahead distances tend to decouple the underactuated dynamics from the actuated dynamics, thus avoiding sway motion (sway and heave motion in 3D).

Remark II.6. The bounds (7-8) show that the disturbances V_x , V_y and κ_v shrink the upper bound for $\sigma > 0$ and increase the lower bound for $\Delta > 0$. These changes can be compensated by increasing the relative velocity of the vessel U_{rd} .

D. Proof of Theorem II.1

In this subsection the proof of Theorem II.1 is given. The proof is inspired by [34]. The dynamics of the cross track error y and the relative sway velocity v_r have to be analyzed. The $y - v_r$ system is obtained combining (1b), (1c) and (6b):

$$\dot{y}_{\text{int}} = \frac{\Delta y}{(y + \sigma y_{\text{int}})^2 + \Delta^2}, \quad (10a)$$

$$\dot{y} = U_{rd} \sin(\psi_d) + v_r \cos(\psi_d) + V_y, \quad (10b)$$

$$\dot{v}_r = X(U_{rd})\dot{\psi}_d + Y(U_{rd})v_r + \kappa_v(\gamma_e) \sin(\beta_e - \psi_d). \quad (10c)$$

Since $\sin(\psi_d) = -(y + \sigma y_{\text{int}})/\sqrt{(y + \sigma y_{\text{int}})^2 + \Delta^2}$ and $\cos(\psi_d) = \Delta/\sqrt{(y + \sigma y_{\text{int}})^2 + \Delta^2}$, (10) becomes:

$$\dot{y}_{\text{int}} = \frac{\Delta y}{(y + \sigma y_{\text{int}})^2 + \Delta^2}, \quad (11a)$$

$$\dot{y} = -U_{rd} \frac{y + \sigma y_{\text{int}}}{\sqrt{(y + \sigma y_{\text{int}})^2 + \Delta^2}} + \frac{\Delta}{\sqrt{(y + \sigma y_{\text{int}})^2 + \Delta^2}} v_r + V_y, \quad (11b)$$

$$\dot{v}_r = X(U_{rd})\dot{\psi}_d + Y(U_{rd})v_r + \kappa_v(\gamma_e) \sin(\beta_e - \psi_d). \quad (11c)$$

The calculation of the equilibrium point of the system (10) yields the following equation:

$$s\sqrt{s^2 + 1} = \frac{V_y}{U_{rd}} s^2 + \frac{\cos(\beta_e)s + \sin(\beta_e)}{U_{rd}|Y^{U_{rd}}|} \kappa_v^{\text{eq}}(s) + \frac{V_y}{U_{rd}}, \quad (12)$$

where $s \triangleq \sigma y_{\text{int}}^{\text{eq}}/\Delta$ and $y_{\text{int}}^{\text{eq}}$ is the value of y_{int} at equilibrium. The term $\kappa_v^{\text{eq}}(s)$ is defined as the value of $\kappa_v(\gamma_e)$ at equilibrium, i.e. when $\gamma_e = \gamma_e^{\text{eq}} \triangleq -\tan^{-1}(s) - \beta_e - \pi$. The equilibrium point equation (12) is a generalized case of similar equations found in [40]–[42], [51]. It has to be shown that (12) has a unique real solution to have a single equilibrium point. The following Lemma gives the sufficient conditions for (12) to have a unique real solution:

Lemma II.1. *If Assumptions II.3 and II.5 hold, then (12) has exactly one real solution $s = \sigma y_{\text{int}}^{\text{eq}}/\Delta$.*

Proof. The proof of Lemma II.1 is given in Appendix A. \square

At equilibrium $y^{\text{eq}} = 0$ while $y_{\text{int}}^{\text{eq}}$ and v_r^{eq} are constant values where $y_{\text{int}}^{\text{eq}}$ is the unique solution of (12) and v_r^{eq} relates to $y_{\text{int}}^{\text{eq}}$ as:

$$v_r^{\text{eq}} = U_{rd} \frac{\sigma y_{\text{int}}^{\text{eq}}}{\Delta} - V_y \sqrt{\left(\frac{\sigma y_{\text{int}}^{\text{eq}}}{\Delta}\right)^2 + 1} \quad (13)$$

The heading angle held by the vessel at steady-state is then $\psi_{ss} \triangleq -\tan^{-1}(\sigma y_{\text{int}}^{\text{eq}}/\Delta)$. A new set of variables is introduced to move the equilibrium point to the origin:

$$e_1 \triangleq y_{\text{int}} - y_{\text{int}}^{\text{eq}}, \quad (14) \quad e_2 \triangleq y + \sigma e_1, \quad (15) \quad e_3 \triangleq v_r - v_r^{\text{eq}}. \quad (16)$$

Taking the time derivatives of (14-16) and using (11), and (13) the transformed dynamics become:

$$\dot{e}_1 = \frac{\Delta(e_2 - \sigma e_1)}{(e_2 + \sigma y_{\text{int}}^{\text{eq}})^2 + \Delta^2}, \quad (17a)$$

$$\begin{aligned} \dot{e}_2 = & -\frac{\sigma^2 \Delta e_1}{(e_2 + \sigma y_{\text{int}}^{\text{eq}})^2 + \Delta^2} + \frac{\Delta e_3}{\sqrt{(e_2 + \sigma y_{\text{int}}^{\text{eq}})^2 + \Delta^2}} \\ & - \left[U_{rd} - \frac{\sigma \Delta}{\sqrt{(e_2 + \sigma y_{\text{int}}^{\text{eq}})^2 + \Delta^2}} \right] \frac{e_2}{\sqrt{(e_2 + \sigma y_{\text{int}}^{\text{eq}})^2 + \Delta^2}} \\ & + V_y f(e_2), \end{aligned} \quad (17b)$$

$$\begin{aligned} \dot{e}_3 = & X(U_{rd})\dot{\psi}_d + Y(U_{rd})e_3 + \frac{\kappa_v(\gamma_e) \cos(\beta_e) e_2}{\sqrt{(e_2 + \sigma y_{\text{int}}^{\text{eq}})^2 + \Delta^2}} \\ & + \sin(\psi_{ss} - \beta_e) g(e_2), \end{aligned} \quad (17c)$$

where $f(e_2)$ is defined as:

$$f(e_2) \triangleq 1 - \frac{\sqrt{(\sigma y_{\text{int}}^{\text{eq}})^2 + \Delta^2}}{\sqrt{(e_2 + \sigma y_{\text{int}}^{\text{eq}})^2 + \Delta^2}}, \quad (18)$$

and $g(e_2)$ is defined as:

$$g(e_2) \triangleq \kappa_v^{\text{eq}} - \kappa_v(\gamma_e) \frac{\sqrt{(\sigma y_{\text{int}}^{\text{eq}})^2 + \Delta^2}}{\sqrt{(e_2 + \sigma y_{\text{int}}^{\text{eq}})^2 + \Delta^2}}. \quad (19)$$

Notice that the following bound holds for $f(e_2)$:

$$|f(e_2)| \leq \frac{|e_2|}{\sqrt{(e_2 + \sigma y_{\text{int}}^{\text{eq}})^2 + \Delta^2}}. \quad (20)$$

One can prove that (20) holds by squaring both sides of the inequality two consecutive times. Furthermore, as a direct consequence of Assumption II.4, the following bound holds for $g(e_2)$:

$$|g(e_2)| \leq \kappa_v^{\text{max}} \frac{|e_2|}{\sqrt{(e_2 + \sigma y_{\text{int}}^{\text{eq}})^2 + \Delta^2}}. \quad (21)$$

Now, substituting for $\dot{\psi}_d$ in (17c) by taking the time derivative of (6a) and inserting the derivatives given by (17a-17b), yields the following form for the system (17):

$$\begin{bmatrix} \dot{e}_1 \\ \dot{e}_2 \\ \dot{e}_3 \end{bmatrix} = \mathbf{A}_1(e_2) \begin{bmatrix} e_1 \\ e_2 \\ e_3 \end{bmatrix} + \mathbf{B}_1(e_2). \quad (22)$$

$\mathbf{A}_1(e_2)$ is given in (24) while $\mathbf{B}_1(e_2)$ is:

$$\mathbf{B}_1(e_2) \triangleq \begin{bmatrix} V_y f(e_2) \\ -\frac{\Delta X^{U_{rd}} V_y}{(e_2 + \sigma y_{\text{int}}^{\text{eq}})^2 + \Delta^2} f(e_2) + \sin(\psi_{ss} - \beta_e) g(e_2) \end{bmatrix}. \quad (23)$$

Lemma II.2 states the stability properties of (22):

Lemma II.2. *Under the conditions of Theorem II.1, the system (22) is UGAS and ULES.*

Proof. The proof of Lemma II.2 is given in Appendix B. \square

Lemma II.2 concludes UGAS and ULES stability for the origin of (22). It is hence possible to conclude that the control objectives (4-5) are achieved with exponential convergence properties in any ball of initial conditions. This is further elaborated on in the analysis in [52] which formally proves that the system is USGES.

Remark II.7. Notice that the UGAS and ULES stability properties of (22) provides this system with a certain robustness with respect to perturbations [53, Lemma 9.1]. This makes the ILOS guidance law (6) potentially very reliable under Assumptions II.1-II.5. Such robustness with respect to perturbations is exploited in the following part where the actuated dynamics are added into the analysis yielding cascaded configurations.

Remark II.8. The value $y_{\text{int}}^{\text{eq}}$ makes sure that, at equilibrium, the vessel holds the heading $\psi_{ss} = -\tan^{-1}(\sigma y_{\text{int}}^{\text{eq}}/\Delta)$ which is the only real solution of (12), i.e. ψ_{ss} is the only possible heading that guarantees path following and compensates for the disturbances.

E. Conclusions

In this part of the paper explicit bounds for the choice of the look-ahead distance and the integral gain of the ILOS guidance scheme have been derived by including the underactuated dynamics into the Lyapunov analysis. Disturbances in the form of constant irrotational ocean currents and constant dynamic, attitude dependent, forces have been also taken into account, while the actuated dynamics have not been considered. The stability analysis reveals UGAS and ULES stability properties for the guidance closed loop system. This guarantees that the guidance closed loop system has a certain robustness with respect to perturbations. Such robustness with respect to perturbations is exploited in the following section where the actuated dynamics are added into the analysis in a cascaded configuration.

$$\mathbf{A}_1(e_2) \triangleq \begin{bmatrix} -\frac{\sigma\Delta}{(e_2+\sigma y_{\text{int}}^{\text{eq}})^2+\Delta^2} & \frac{\Delta}{(e_2+\sigma y_{\text{int}}^{\text{eq}})^2+\Delta^2} & 0 \\ -\frac{\sigma^2\Delta}{(e_2+\sigma y_{\text{int}}^{\text{eq}})^2+\Delta^2} & -\frac{U_{rd}}{\sqrt{(e_2+\sigma y_{\text{int}}^{\text{eq}})^2+\Delta^2}} + \frac{\sigma\Delta}{(e_2+\sigma y_{\text{int}}^{\text{eq}})^2+\Delta^2} & \frac{\Delta}{\sqrt{(e_2+\sigma y_{\text{int}}^{\text{eq}})^2+\Delta^2}} \\ \frac{\sigma^2\Delta^2 X^{Urd}}{((e_2+\sigma y_{\text{int}}^{\text{eq}})^2+\Delta^2)^2} & \frac{U_{rd}\Delta X^{Urd}}{((e_2+\sigma y_{\text{int}}^{\text{eq}})^2+\Delta^2)^{3/2}} - \frac{\sigma\Delta^2 X^{Urd}}{((e_2+\sigma y_{\text{int}}^{\text{eq}})^2+\Delta^2)^2} + \frac{\kappa_v(\gamma_e)\cos(\beta_e)}{\sqrt{(e_2+\sigma y_{\text{int}}^{\text{eq}})^2+\Delta^2}} & Y^{Urd} - \frac{\Delta^2 X^{Urd}}{((e_2+\sigma y_{\text{int}}^{\text{eq}})^2+\Delta^2)^{3/2}} \end{bmatrix} \quad (24)$$

III. PATH FOLLOWING CONTROL OF UNDERACTUATED AUVS IN THE PRESENCE OF OCEAN CURRENTS

In this part of the paper a 3D version of the ILOS guidance law is presented and the sway and heave underactuated dynamics as well as the surge, pitch and yaw actuated dynamics are included in the analysis of the closed loop system. The results from Section II are hence extended to underactuated AUVs for 3D straight line path following applications in the presence of constant irrotational ocean currents, acting in any direction of the inertial frame. The 3D ILOS guidance law with integral action in both the vertical and horizontal directions is shown to solve the task together with three feedback controllers in a cascaded configuration. The dynamics of the AUV are expressed in terms of its relative velocity, that is the velocity of the vessel with respect to the water. This is possible since the current is assumed constant and irrotational in the inertial frame [10], [54]. The closed loop stability analysis shows UGAS and ULES for the origin of the closed loop system, and explicit bounds on the guidance law parameters are given to guarantee stability.

The following sub-sections are organized as follows: Section III-A presents the model of the vehicle and Section III-B identifies the control objective. Section III-C presents the strategy that solves the path following task defined in Section III-B. The main result including the stability conditions is given in Section III-D and proven in Section III-E. Conclusions are given in Section III-F.

A. The Control Plant Model

1) Model Assumptions:

Assumption III.1. The body-fixed coordinate frame b is located in a point $(x_g^*, 0, 0)$ from the vehicle's center of gravity (CG) along the center-line of the vessel, where x_g^* is to be defined later.

Assumption III.2. The roll motion is passively stabilized through fins or by gravity and therefore can be neglected. Hence, the motion of the vehicle is described in 5 degrees of freedom (DOF), that is surge, sway, heave, pitch and yaw.

Assumption III.3. The vehicle is neutrally buoyant and the center of gravity (CG) and the center of buoyancy (CB) are located along the same vertical axis in b .

Assumption III.4. The AUV is xz plane symmetric and has a large length-to-width ratio.

Assumption III.5. The surge mode is decoupled from the other degrees of freedom and only dominating interconnections between sway and yaw, and between heave and pitch are considered.

Remark III.1. Assumptions III.2, III.3, III.4 and III.5 are common assumptions in maneuvering control of slender body AUVs [10]. They also hold for the LAUV and HUGIN vehicles [31], [55].

Assumption III.6. The hydrodynamic damping is considered linear.

Remark III.2. For low speed maneuvering, Assumption III.6 is a mild assumption as any non-linear damping should enhance the directional stability of the vehicle due to the passive nature of the hydrodynamic damping forces.

Assumption III.7. The ocean current in the inertial frame i , $\mathbf{V}_c \triangleq [V_x, V_y, V_z]^T$, is constant, irrotational and bounded. Hence, there exists a $V_{\max} > 0$ such that $V_{\max} \geq \sqrt{V_x^2 + V_y^2 + V_z^2}$.

2) *The Vehicle Control Model:* Following Assumption III.2 the state of the underwater vehicle is given by the vector $\boldsymbol{\eta} \triangleq [x, y, z, \theta, \psi]^T$ which describes the position and the orientation of the AUV with respect to the inertial frame i . In particular, θ is the vehicle pitch angle and ψ is the vehicle yaw angle. The vector $\boldsymbol{\nu} \triangleq [u, v, w, q, r]^T$ contains the linear and angular velocities of the vehicle defined in the body-fixed frame b where u is the surge velocity, v is the sway velocity, w is the heave velocity, q is the pitch rate and r is the yaw rate. According to Assumption III.7 the ocean current is irrotational in i and its velocity in the body frame b , $\boldsymbol{\nu}_c \triangleq [u_c, v_c, w_c, 0, 0]^T$, is obtained from $[u_c, v_c, w_c]^T = \mathbf{R}^T(\theta, \psi)\mathbf{V}_c$ where $\mathbf{R}(\theta, \psi)$ is the rotation matrix from b to i , defined using the zyx convention [10]. Furthermore, the fact that $\dot{\mathbf{V}}_c = \mathbf{0}$ gives $\dot{\boldsymbol{\nu}}_c = [rv_c - qw_c, -ru_c, qu_c, 0, 0]^T$. Also for the AUV case it is useful to introduce the relative velocity, defined as the velocity of the vehicle with respect to the flow: $\boldsymbol{\nu}_r \triangleq \boldsymbol{\nu} - \boldsymbol{\nu}_c = [u_r, v_r, w_r, q, r]^T$. The vector $\boldsymbol{\nu}_r$ is defined in b where u_r is the relative surge velocity, v_r is the relative sway velocity and w_r is the relative heave velocity. It is shown in [10] that since the ocean current is constant and irrotational in i , the underwater vehicle can be described by the following 5-DOF maneuvering model:

$$\dot{\boldsymbol{\eta}} = \mathbf{J}(\boldsymbol{\eta})\boldsymbol{\nu}_r + [\mathbf{V}_c^T, 0, 0]^T, \quad (25)$$

$$\mathbf{M}\dot{\boldsymbol{\nu}}_r + \mathbf{C}(\boldsymbol{\nu}_r)\boldsymbol{\nu}_r + \mathbf{D}\boldsymbol{\nu}_r + \mathbf{g}(\boldsymbol{\eta}) = \mathbf{B}\mathbf{f}. \quad (26)$$

The vector $\mathbf{f} \triangleq [T_u, T_q, T_r]^T$ is the control input vector, containing the surge thrust (T_u), the pitch rudder angle (T_q) and the yaw rudder angle (T_r). The dimension of the control input vector \mathbf{f} is two less than the DOFs of the vessel, therefore the model (26) is underactuated in its configuration space. The term $\mathbf{J}(\boldsymbol{\eta})$ is the velocity transformation matrix defined as;

$$\mathbf{J}(\boldsymbol{\eta}) \triangleq \begin{bmatrix} \mathbf{R}(\theta, \psi) & \mathbf{0} \\ \mathbf{0} & \mathbf{T}(\theta) \end{bmatrix}, \quad (27)$$

where $\mathbf{T}(\theta) \triangleq \text{diag}(1, 1/\cos(\theta))$, $|\theta| \neq \frac{\pi}{2}$.

Remark III.3. Given the singularity in θ , the open loop system (25-26) can be considered as stabilizable forward-complete [56] since the global stability results refer to the closed loop system, where no singularity is present (Section III-E).

The matrix $\mathbf{M} = \mathbf{M}^T > 0$ is the mass and inertia matrix, and includes hydrodynamic added mass. The matrix \mathbf{C} is the Coriolis and centripetal matrix, $\mathbf{D} > 0$ is the hydrodynamic damping matrix and $\mathbf{B} \in \mathbb{R}^{5 \times 3}$ is the actuator configuration matrix. Following Assumption III.3, the gravity vector in CG can be written as $\mathbf{g}(\boldsymbol{\eta}) \triangleq [0, 0, 0, BG_z W \sin(\theta), 0]^T$, where BG_z is the vertical distance between CG and CB, and W is the weight of the vehicle. For manoeuvring control purposes, the matrices $\mathbf{R}(\theta, \psi)$, \mathbf{M} , \mathbf{D} and \mathbf{B} are:

$$\mathbf{R} \triangleq \begin{bmatrix} c\psi c\theta & -s\psi & c\psi s\theta \\ s\psi c\theta & c\psi & s\psi s\theta \\ -s\theta & 0 & c\theta \end{bmatrix}, \quad \mathbf{D} \triangleq \begin{bmatrix} d_{11} & 0 & 0 & 0 & 0 \\ 0 & d_{22} & 0 & 0 & d_{25} \\ 0 & 0 & d_{33} & d_{34} & 0 \\ 0 & 0 & d_{43} & d_{44} & 0 \\ 0 & d_{52} & 0 & 0 & d_{55} \end{bmatrix}, \quad (28)$$

$$\mathbf{B} \triangleq \begin{bmatrix} b_{11} & 0 & 0 \\ 0 & 0 & b_{23} \\ 0 & b_{32} & 0 \\ 0 & b_{42} & 0 \\ 0 & 0 & b_{53} \end{bmatrix}, \quad \mathbf{M} \triangleq \begin{bmatrix} m_{11} & 0 & 0 & 0 & 0 \\ 0 & m_{22} & 0 & 0 & m_{25} \\ 0 & 0 & m_{33} & m_{34} & 0 \\ 0 & 0 & m_{34} & m_{44} & 0 \\ 0 & m_{25} & 0 & 0 & m_{55} \end{bmatrix},$$

where $s \triangleq \sin(\cdot)$ and $c \triangleq \cos(\cdot)$. The Coriolis and centripetal matrix \mathbf{C} is obtained from \mathbf{M} as described in [10]. The particular structure of \mathbf{M} and \mathbf{D} is justified by Assumptions III.2-III.6. The actuator configuration matrix \mathbf{B} has full column rank and maps the control inputs T_u , T_q and T_r into forces and moments acting on the vessel. Finally, x_g^* from Assumption III.1 is chosen so that $\mathbf{M}^{-1}\mathbf{B}\mathbf{f} = [\tau_u, 0, 0, \tau_q, \tau_r]^T$. The point $(x_g^*, 0, 0)$ exists for all AUVs of cylindrical shape employing symmetric steering and diving control surfaces [31], [57].

Remark III.4. The model used in [57] contains the velocity vector \mathbf{v} as well as the relative velocity vector \mathbf{v}_r . This complicates the controller design and weakens the cascade configuration, resulting in weaker stability properties. The model (25-26) overcomes the problem.

3) *The Model in Component Form:* To solve nonlinear underactuated control design problems it is convenient to expand (25-26) into:

$$\dot{x} = u_r c \psi c \theta - v_r s \psi + w_r c \psi s \theta + V_x, \quad (29a)$$

$$\dot{y} = u_r s \psi c \theta + v_r c \psi + w_r s \psi s \theta + V_y, \quad (29b)$$

$$\dot{z} = -u_r s \theta + w_r c \theta + V_z, \quad (29c)$$

$$\dot{\theta} = q, \quad (29d)$$

$$\dot{\psi} = r / c \theta, \quad (29e)$$

$$\dot{u}_r = F_{u_r}(v_r, w_r, r, q) - (d_{11}/m_{11})u_r + \tau_u, \quad (29f)$$

$$\dot{v}_r = X_{v_r}(u_r)r + Y_{v_r}(u_r)v_r, \quad (29g)$$

$$\dot{w}_r = X_{w_r}(u_r)q + Y_{w_r}(u_r)w_r + Z_{w_r}s\theta, \quad (29h)$$

$$\dot{q} = F_q(\theta, u_r, w_r, q) + \tau_q, \quad (29i)$$

$$\dot{r} = F_r(u_r, v_r, r) + \tau_r. \quad (29j)$$

The expressions F_{u_r} , X_{v_r} , Y_{v_r} , X_{w_r} , Y_{w_r} , Z_{w_r} , F_q and F_r are given in Appendix C. Notice that the functions $X_{v_r}(u_r)$, $X_{w_r}(u_r)$, $Y_{v_r}(u_r)$ and $Y_{w_r}(u_r)$ are bounded for bounded arguments. An additional key assumption is introduced:

Assumption III.8. The functions $Y_{v_r}(u_r)$ and $Y_{w_r}(u_r)$ satisfy:

$$Y_a(u_r) \leq -Y_a^{\min} < 0, \quad \forall u_r \in [-V_{\max}, U_{rd}], \quad a \in \{v_r, w_r\}.$$

Remark III.5. Assumption III.8 is justified by the following contradiction: $Y_{v_r}(u_r) \geq 0$ and $Y_{w_r}(u_r) \geq 0$ would imply an undamped or nominally unstable vehicle in sway and heave which is not the case in practice [31]. This assumption is thus linked to the straight-line stability properties of the AUV. Notice that no bounds are implied on u_r while $U_{rd} > 0$ will be defined later.

B. The Control Objective

The control system should make the vehicle follow a given straight line \mathcal{P} and maintain a desired constant surge relative velocity $U_{rd} > 0$ in the presence of unknown constant and irrotational ocean currents. The inertial reference frame i is placed such that the z -axis points down and the x -axis is aligned with the desired path \mathcal{P} as shown in Fig. 2. This simplifies the control problem without any loss of generality. The desired path \mathcal{P} is then defined as $\mathcal{P} \triangleq \{(x, y, z) \in \mathbb{R}^3 : y = 0, z = 0\}$. Hence, the y and z coordinates of the vehicle correspond to the horizontal and vertical cross-track errors and the objectives the control system should pursue can be formalized as:

$$\lim_{t \rightarrow \infty} y(t) = 0, \quad \lim_{t \rightarrow \infty} z(t) = 0, \quad (30) \quad (31)$$

$$\lim_{t \rightarrow \infty} \psi(t) = \psi_{ss}, \quad \lim_{t \rightarrow \infty} \theta(t) = \theta_{ss}, \quad \lim_{t \rightarrow \infty} u_r(t) = U_{rd}, \quad (32) \quad (33) \quad (34)$$

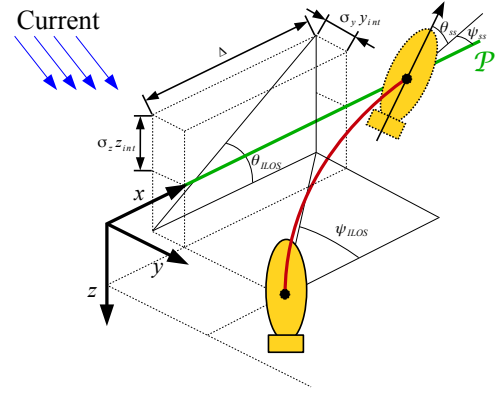


Fig. 2. Integral line of sight guidance for an underactuated underwater vehicle, in this case $\Delta_y = \Delta_z = \Delta$. At steady state the angles ψ_{ss} and θ_{ss} allow the underactuated AUV to counteract the current.

where $\theta_{ss} \in (-\frac{\pi}{2}, \frac{\pi}{2})$ as well as $\psi_{ss} \in (-\frac{\pi}{2}, \frac{\pi}{2})$ are constants. The yaw angle $\psi(t)$ and the pitch angle $\theta(t)$ are not required to converge to zero but rather to steady-state constant values since the AUV is required to pitch and crab in order not to drift away. The values of ψ_{ss} and θ_{ss} will be specified later.

Remark III.6. Notice that non horizontal motion can also be considered. Non horizontal motion affects the gravity vector $\mathbf{g}(\eta)$ where gravity is represented by the term $Z_{w_r} \sin(\theta)$ in (29h). In particular, this term is seen as an additional bounded constant disturbance in heave that the guidance system compensates for as well (see Section III-E).

Remark III.7. In this paper the AUV is required to hold a constant surge relative velocity U_{rd} as stated in (34), while in [34] and [57] the vehicle is required to follow \mathcal{P} with a constant speed $U_d > 0$. The path following speed is therefore not directly controlled but results instead from the relative speed and the current velocity. Even if this is not ideal for speed profile planning/tracking scenarios, controlling the relative velocity of the vessel gives direct control over the energy consumption, since the hydrodynamic damping depends on \mathbf{v}_r , and any lift forces due to transom stern effects. Furthermore, relative velocity control removes the unknown term \mathbf{v}_c from the velocity feedback loop. The relative velocity \mathbf{v}_r is measurable via, for example, a Doppler velocity log (DVL) [58].

Finally, the desired relative surge velocity needs to be sufficiently large compared to the ocean current velocity in order to guarantee maneuverability of the AUV. It is later shown that the particular bound given in Assumption III.9 allows the AUV to achieve path following for currents acting in any direction of the 3D space:

Assumption III.9. The desired constant relative surge velocity U_{rd} satisfies the following condition:

$$U_{rd} > \max \left\{ V_{\max} + \frac{5}{2} \left| \frac{Z_{w_r}}{Y_{w_r}(U_{rd})} \right|, 2V_{\max} + 2 \left| \frac{Z_{w_r}}{Y_{w_r}(U_{rd})} \right| \right\},$$

Remark III.8. It is always possible to find values of U_{rd} satisfying Assumption III.9, since $|Y_{w_r}(u_r)|$ is strictly increasing for $u_r > 0$.

C. The Control System

In this section a control strategy to solve the control problem defined in Section III-B is proposed. First, the LOS guidance law is introduced and then the surge, pitch and yaw controllers from [40] are added in a cascaded configuration.

1) *Path Following Control Strategy*: The integral LOS guidance law from [40] is chosen to set the heading and pitch angles, and make the AUV converge and follow the x -axis in presence of ocean currents:

$$\theta_{\text{ILOS}} \triangleq \tan^{-1} \left(\frac{z + \sigma_z z_{\text{int}}}{\Delta_z} \right), \quad \dot{z}_{\text{int}} = \frac{\Delta_z z}{(z + \sigma_z z_{\text{int}})^2 + \Delta_z^2}, \quad (35a) \quad (35b)$$

$$\psi_{\text{ILOS}} \triangleq -\tan^{-1} \left(\frac{y + \sigma_y y_{\text{int}}}{\Delta_y} \right), \quad \dot{y}_{\text{int}} = \frac{\Delta_y y}{(y + \sigma_y y_{\text{int}})^2 + \Delta_y^2}, \quad (35c) \quad (35d)$$

where the look-ahead distances in the vertical and horizontal planes $\Delta_z > 0$ and $\Delta_y > 0$, as well as the integral gains $\sigma_y > 0$ and $\sigma_z > 0$, are constant design parameters. A graphical explanation of the integral LOS is given in Fig. 2. The guidance law (35) is a 3D extension of the (6) guidance law and a detailed discussion of the properties of the ILOS guidance law is given in Section II-B. Finally, notice that the controller has the minimum number of integral actions to guarantee the achievement of (30-34) since there are three regulated outputs ($y(t)$, $z(t)$ and $u_r(t)$), three unknown terms (V_x , V_y and V_z) and two integrators (35b, 35d).

2) *The Surge, Pitch and Yaw Controllers*: According to (34), the relative surge velocity of the vessel u_r should follow the desired value $u_{rd}(t) = U_{rd}$. Therefore, to track $u_{rd}(t)$ the following controller is used:

$$\tau_u = -F_{u_r}(v_r, w_r, r, q) + \frac{d_{11}}{m_{11}} u_{rd} + \dot{u}_{rd} - k_{u_r}(u_r - u_{rd}). \quad (36)$$

The gain $k_{u_r} > 0$ is constant. The controller (36) is a feedback linearizing P-controller that in a closed loop configuration with (29f) guarantees exponential tracking of $u_{rd}(t)$. Damping is not canceled to provide some robustness with respect to model uncertainties. The following controller is used to track the desired pitch angle $\theta_d \triangleq \theta_{\text{ILOS}}$:

$$\tau_q = -F_q(\theta, u_r, w_r, q) + \ddot{\theta}_d - k_\theta(\theta - \theta_d) - k_q(\dot{\theta} - \dot{\theta}_d), \quad (37)$$

where $k_\theta, k_q > 0$ are constant gains. The controller (37) is a feedback linearizing PD controller that in a closed loop configuration with (29d)-(29i) makes sure that θ and q exponentially track θ_d and $\dot{\theta}_d$ respectively. Finally, the following feedback linearizing PD-controller is used to track the desired yaw angle $\psi_d \triangleq \psi_{\text{ILOS}}$:

$$\tau_r = -F_r(u_r, v_r, r) - q \sin(\theta) \dot{\psi} + \cos(\theta) \left[\ddot{\psi}_d - k_\psi(\psi - \psi_d) - k_r(\dot{\psi} - \dot{\psi}_d) \right]. \quad (38)$$

The parameters $k_\psi, k_r > 0$ are constant gains and the yaw control law (38), in a closed loop configuration with (29e)-(29j), guarantees exponential convergence of ψ and $\dot{\psi}$ to ψ_d and $\dot{\psi}_d$ respectively.

Remark III.9. The controllers (36), (37) and (38) are feedback linearizing controllers, hence if the model suffers from high uncertainty other approaches should be considered. It can be seen in the following stability analysis that any control law that gives UGES or UGAS and ULES of the fully actuated dynamics will give the derived stability result.

Remark III.10. The closed loop system given by the controller (38) in combination with (29e)-(29j) does not have singularities since the limits of $\cos(\theta)/\cos(\theta)$ and $\cos^2(\theta)/\cos^2(\theta)$ for $\theta \rightarrow \pi/2 + k\pi$ exist and equal 1 [31]. Hence, the open loop system (25-26) can be considered as stabilizable forward complete [56].

D. Stability Conditions

This section presents the main result of this chapter, including the conditions under which the proposed control law achieves (30-34).

The abbreviations $X_a^{U_{rd}} \triangleq X_a(U_{rd})$ and $Y_a^{U_{rd}} \triangleq Y_a(U_{rd})$ are used, where $a \in \{v_r, w_r\}$.

Theorem III.1. *Given an underactuated underwater vehicle described by the dynamical system (29). If Assumptions III.7-III.9 hold and if the look-ahead distances Δ_y, Δ_z satisfy the conditions:*

$$\Delta_y > \frac{|X_{v_r}^{U_{rd}}|}{|Y_{v_r}^{U_{rd}}|} \left[\frac{5 \Gamma_{\max} + V_{\max} + \sigma_y}{4 \Gamma_{\inf} - V_{\max} - \sigma_y} + 1 \right], \quad (39)$$

$$\Delta_z > \frac{|X_{w_r}^{U_{rd}}|}{|Y_{w_r}^{U_{rd}}|} \rho(\sigma_z) \left[\frac{5 U_{rd} + V_{\max} + \sigma_z}{4 U_{rd} - V_{\max} - \sigma_z} + 1 \right], \quad (40)$$

where the integral gains σ_y, σ_z satisfy:

$$0 < \sigma_y < \Gamma_{\inf} - V_{\max}, \quad (41)$$

$$0 < \sigma_z < U_{rd} - V_{\max} - \frac{5}{2} \left| \frac{Z_{w_r}}{Y_{w_r}^{U_{rd}}} \right|, \quad (42)$$

then the controllers (36-38) and the guidance law (35) with $u_{rd}(t) = U_{rd}$ guarantee achievement of the control objectives (30-34). The control objectives (32-33) are fulfilled with $\psi_{ss} = -\tan^{-1}(V_y/\sqrt{\Gamma(s)^2 - V_y^2})$ and $\theta_{ss} = \tan^{-1}(s)$.

Remark III.11. The constant s is defined in Section III-E. The constants $\Gamma_{\max}, \Gamma_{\inf}$ and the functions $\Gamma(s), \rho(\sigma_z)$ are given in (43-45). It is shown in Section III-E that s is such that $\Gamma_{\inf} < \Gamma(s) \leq \Gamma_{\max}$. Notice that $\Gamma_{\inf} > 0$ as long as Assumption III.9 is satisfied.

$$\Gamma(s) \triangleq U_{rd} \frac{1}{\sqrt{s^2 + 1}} - \frac{Z_{w_r}}{Y_{w_r}^{U_{rd}}} \frac{s^2}{s^2 + 1}, \quad (43)$$

$$\Gamma_{\inf} \triangleq \frac{3}{5} \left[U_{rd} - \left| \frac{Z_{w_r}}{Y_{w_r}^{U_{rd}}} \right| \right], \quad \Gamma_{\max} \triangleq U_{rd}, \quad (44)$$

$$\rho(\sigma_z) \triangleq \frac{U_{rd} - V_{\max} - \sigma_z}{U_{rd} - V_{\max} - \sigma_z - \frac{5}{2} \left| \frac{Z_{w_r}}{Y_{w_r}^{U_{rd}}} \right|}. \quad (45)$$

E. Proof of Theorem III.1

The actuated dynamics (29f), (29i) and (29j) of the AUV in closed loop configuration with the controllers (36-38) are considered first. Given the vector $\zeta \triangleq [\tilde{u}_r, \tilde{\theta}, \tilde{\psi}, \tilde{\psi}]^T$ where $\tilde{u}_r \triangleq u_r - U_{rd}$, $\tilde{\theta} \triangleq \theta - \theta_d$, $\tilde{\psi} \triangleq \psi - \psi_d$ and $\tilde{\psi} \triangleq \dot{\psi} - \dot{\psi}_d$, the dynamics of ζ are obtained by combining the system equations (29d), (29e), (29f), (29i) and (29j) with the control laws (36-38):

$$\dot{\zeta} = \begin{bmatrix} -k_{u_r} - \frac{d_{11}}{m_{11}} & 0 & 0 & 0 & 0 \\ 0 & 0 & -k_\theta & 0 & 0 \\ 0 & -k_\theta & -k_q & 0 & 0 \\ 0 & 0 & 0 & 0 & 1 \\ 0 & 0 & 0 & -k_\psi & -k_r \end{bmatrix} \zeta \triangleq \Sigma \zeta. \quad (46)$$

The system (46) is linear and time-invariant. Furthermore, the gains $k_{u_r}, k_\theta, k_q, k_\psi, k_r$ and the term $\frac{d_{11}}{m_{11}}$ are all strictly positive. Therefore the matrix Σ is Hurwitz and the origin $\zeta = \mathbf{0}$ of (46) is UGES. Hence, $u(t) \rightarrow u_{rd}(t)$, $\theta(t) \rightarrow \theta_d(t)$ and $\psi(t) \rightarrow \psi_d(t)$ exponentially. As a result, the control goal (34) is achieved with exponential converging properties in any ball of initial conditions.

The dynamics of the cross track error z and the relative heave velocity w_r are analyzed next. The $z - w_r$ subsystem is obtained combining (29c), (29h) and (35b):

$$\dot{z}_{\text{int}} = \frac{\Delta_z z}{(z + \sigma_z z_{\text{int}})^2 + \Delta_z^2}, \quad (47)$$

$$\dot{z} = -u_r \sin(\tilde{\theta} + \theta_d) + w_r \cos(\tilde{\theta} + \theta_d) + V_z, \quad (48)$$

$$\dot{w}_r = X_{w_r}(\tilde{u}_r + U_{rd})(\tilde{\theta} + \dot{\theta}_d) + Y_{w_r}(\tilde{u}_r + U_{rd})w_r + Z_{w_r} \sin(\tilde{\theta} + \theta_d). \quad (49)$$

The calculation of the equilibrium point of the system (47-49) on the manifold $\zeta = \mathbf{0}$ yields the following equation:

$$s\sqrt{s^2+1} = \frac{V_z}{U_{rd}}s^2 - \frac{Z_{w_r}}{U_{rd}Y_{w_r}^{U_{rd}}}s + \frac{V_z}{U_{rd}}, \quad (50)$$

where $s \triangleq \sigma_z z_{\text{int}}^{\text{eq}}/\Delta_z$ and $z_{\text{int}}^{\text{eq}}$ is the value of z_{int} at equilibrium. It has to be shown that (50) has a unique real solution to have a single equilibrium point. The following Lemma gives the sufficient conditions for (50) to have a unique real solution:

Lemma III.1. *If Assumption III.9 holds then (50) has exactly one real solution $s = \sigma_z z_{\text{int}}^{\text{eq}}/\Delta_z$.*

Proof. Equation (50) is a simplification of (12). Therefore, applying Lemma III.1 from Appendix A, it is possible to conclude that (50) has a unique real solution. \square

At equilibrium $z^{\text{eq}} = 0$ while $z_{\text{int}}^{\text{eq}}$ and w_r^{eq} are constant values where $z_{\text{int}}^{\text{eq}}$ is the unique solution of (50) and w_r^{eq} relates to $z_{\text{int}}^{\text{eq}}$ as:

$$w_r^{\text{eq}} = U_{rd} \frac{\sigma_z z_{\text{int}}^{\text{eq}}}{\Delta_z} - V_z \sqrt{\left(\frac{\sigma_z z_{\text{int}}^{\text{eq}}}{\Delta_z}\right)^2 + 1}. \quad (51)$$

The pitch angle held by the AUV at steady state is then $\theta_{ss} = \tan^{-1}(s) = \tan^{-1}(\sigma_z z_{\text{int}}^{\text{eq}}/\Delta_z)$. Before proceeding with the analysis of the system (47-49) another consequence of Assumption III.9 is considered. As long as Assumption III.9 is satisfied, the following bound holds:

$$\left| \frac{V_z}{U_{rd}}s^2 - \frac{Z_{w_r}}{U_{rd}Y_{w_r}^{U_{rd}}}s + \frac{V_z}{U_{rd}} \right| < \frac{1}{2}(s^2 + |s| + 1). \quad (52)$$

It is seen that a bound $s_{\text{sup}} > |s|$ can be found by setting the upper bound (52) equal to $|s|\sqrt{s^2+1}$:

$$\left| s_{\text{sup}} \sqrt{s_{\text{sup}}^2 + 1} \right| = \frac{1}{2}(s_{\text{sup}}^2 + |s_{\text{sup}}| + 1). \quad (53)$$

Solving (53) for $s_{\text{sup}} > 0$ gives the only accepted real positive solution $s_{\text{sup}} \approx 1.13$. Therefore, it is straightforward to verify that $\Gamma_{\text{inf}} < \Gamma(s_{\text{sup}}) \leq \Gamma(s)$, where Γ_{inf} and $\Gamma(s)$ were defined in (43-44). At this point a new set of variables is introduced to move the equilibrium of (47-49) to the origin:

$$e_{z1} \triangleq z_{\text{int}} - z_{\text{int}}^{\text{eq}}, \quad e_{z2} \triangleq z + \sigma_z e_{z1}, \quad e_{z3} \triangleq w_r - w_r^{\text{eq}}. \quad (54)$$

Substituting (35a) for θ_d , factorizing the result with respect to ζ and applying the transformation (54) leads to the following transformed interconnected dynamics:

$$\begin{bmatrix} \dot{e}_{z1} \\ \dot{e}_{z2} \\ \dot{e}_{z3} \end{bmatrix} = \mathbf{A}_2(e_{z2}) \begin{bmatrix} e_{z1} \\ e_{z2} \\ e_{z3} \end{bmatrix} + \mathbf{B}_2(e_{z2}) + \mathbf{H}_2(z, z_{\text{int}}, \theta_d, w_r, \zeta)\zeta, \quad (55a)$$

$$\dot{\zeta} = \Sigma\zeta. \quad (55b)$$

The matrix \mathbf{H}_2 contains all the terms vanishing at $\zeta = \mathbf{0}$. $\mathbf{A}_2(e_{z2})$ is given in (99) of Appendix C while $\mathbf{B}_2(e_{z2})$ and $\mathbf{H}_2(z, z_{\text{int}}, \theta_d, w_r, \zeta)$ are:

$$\mathbf{B}_2 \triangleq \begin{bmatrix} V_z f(e_{z2}) \\ \frac{\Delta_z X_{w_r}^{U_{rd}} V_z f(e_{z2})}{(e_{z2} + \sigma_z z_{\text{int}}^{\text{eq}})^2 + \Delta_z^2} - Z_{w_r} \frac{s}{\sqrt{s^2+1}} f(e_{z2}) \\ 0 \end{bmatrix}, \quad (56)$$

$$\mathbf{H}_2 \triangleq \begin{bmatrix} 0 & 0 \\ \frac{\Delta_z X_{w_r} (\tilde{u}_r + U_{rd})}{(e_{z2} + \sigma_z z_{\text{int}}^{\text{eq}})^2 + \Delta_z^2} & 1 \end{bmatrix} \begin{bmatrix} \mathbf{h}_z^T \\ \mathbf{h}_{w_r}^T \end{bmatrix}, \quad (57)$$

The function $g(e_{y2})$ is identical to $f(e_y)$ given in (18) and thus the bound (20) applies. The vectors $\mathbf{h}_z(\theta_d, w_r, \zeta)$ and $\mathbf{h}_{w_r}(z, z_{\text{int}}, \theta_d, w_r, \zeta)$ are given in Appendix C. The system (55) is a cascaded system, where the linear UGES system (55b) perturbs

the dynamics (55a) through the interconnection matrix \mathbf{H}_2 . The following Lemma states the stability properties of the cascade (55):

Lemma III.2. *Under the conditions of Theorem III.1, the origin of the system (55) is UGAS and ULES.*

Proof. Consider the nominal system defined on $\zeta = \mathbf{0}$:

$$\begin{bmatrix} \dot{e}_{z1} \\ \dot{e}_{z2} \\ \dot{e}_{z3} \end{bmatrix} = \mathbf{A}_2(e_{z2}) \begin{bmatrix} e_{z1} \\ e_{z2} \\ e_{z3} \end{bmatrix} + \mathbf{B}_2(e_{z2}). \quad (58)$$

The system (58) is equivalent to the system (22). Therefore, applying of Lemma II.2 from Appendix B it is possible to conclude UGAS and ULES for the origin of the system (58). Moreover, since the perturbing system (55b) is UGES and the interconnection matrix $\mathbf{H}_2(z, z_{\text{int}}, \theta_d, w_r, \zeta)$ can be shown to satisfy $\|\mathbf{H}_2\| \leq \delta_1(\|\zeta\|)(|z| + |z_{\text{int}}| + |w_r|) + \delta_2(\|\zeta\|)$, where $\delta_1(\cdot)$ and $\delta_2(\cdot)$ are some continuous non-negative functions, applying [59, Theorem 2] and [60, Lemma 8] it is possible to conclude UGAS and ULES for the cascaded system (55). \square

According to Lemma III.2, under the conditions of Theorem III.1, the origin of the system (55) given by $(e_{z1}, e_{z2}, e_{z3}, \zeta) = (0, 0, 0, \mathbf{0})$ is UGAS and ULES. Hence, the control objectives (31) and (33) are achieved with exponential converging properties with $\theta_{ss} = \theta_{ss}^*$ and $\chi \triangleq [e_{z1}, e_{z2}, e_{z3}, \zeta^T]^T$ is a vector of exponentially converging signals.

Finally, the $y - v_r$ subsystem is considered. The AUV dynamics and kinematics form a cascaded system where (55) perturbs the y cross-track error. The $y - v_r$ subsystem is obtained from (29b), (29g) and (35d):

$$\dot{y}_{\text{int}} = \frac{\Delta_y y}{(y + \sigma_y y_{\text{int}})^2 + \Delta_y^2}, \quad (59)$$

$$\dot{y} = u_r \cos(\tilde{\theta} + \theta_d) \sin(\tilde{\psi} + \psi_d) + v_r \cos(\tilde{\psi} + \psi_d) + w_r \sin(\tilde{\psi} + \psi_d) \sin(\tilde{\theta} + \theta_d) + V_y, \quad (60)$$

$$\dot{v}_r = X_{v_r}(\tilde{u}_r + U_{rd})(\tilde{\psi} + \dot{\psi}_d) \cos(\tilde{\theta} + \theta_d) + Y_{v_r}(\tilde{u}_r + U_{rd})v_r. \quad (61)$$

The equilibrium point of the system (59-61) on the manifold $\chi = \mathbf{0}$ is:

$$y_{\text{int}}^{\text{eq}} = \frac{\Delta_y}{\sigma_y} \frac{V_y}{\sqrt{\Gamma(s)^2 - V_y^2}}, \quad y^{\text{eq}} = 0, \quad v_r^{\text{eq}} = 0, \quad (62)$$

where $\Gamma(s)$ is defined in (43). Therefore, a new set of variables is introduced to move the equilibrium point to the origin: $e_{y1} \triangleq y_{\text{int}} - y_{\text{int}}^{\text{eq}}$ and $e_{y2} \triangleq y + \sigma_y e_{y1}$. Substituting (35a) and (35c) for θ_d and ψ_d , factorizing the result with respect to χ and moving the equilibrium point to the origin yields the following interconnected dynamics:

$$\begin{bmatrix} \dot{e}_{y1} \\ \dot{e}_{y2} \\ \dot{v}_r \end{bmatrix} = \mathbf{A}_3(e_{y2}) \begin{bmatrix} e_{y1} \\ e_{y2} \\ v_r \end{bmatrix} + \mathbf{B}_3(e_{y2}) + \mathbf{H}_3(y, y_{\text{int}}, \theta_d, \psi_d, v_r, \chi)\chi, \quad (63a)$$

$$\dot{\chi} = \begin{bmatrix} \mathbf{A}_2(e_{z2}) & \mathbf{H}_2(z, z_{\text{int}}, \theta_d, w_r, \zeta) \\ \mathbf{0} & \Sigma \end{bmatrix} \chi + \begin{bmatrix} \mathbf{B}_2(e_{z2}) \\ \mathbf{0} \end{bmatrix}. \quad (63b)$$

The term \mathbf{H}_3 contains all the terms vanishing at $\chi = \mathbf{0}$. $\mathbf{A}_3(e_{y2})$ is given in (100) of Appendix C while $\mathbf{B}_3(e_{y2})$ and $\mathbf{H}_3(y, y_{\text{int}}, \theta_d, \psi_d, v_r, \chi)$ are defined as:

$$\mathbf{B}_3 \triangleq \begin{bmatrix} V_y g(e_{y2}) \\ -\frac{1}{\sqrt{s^2+1}} \frac{\Delta_y X_{v_r}^{U_{rd}} V_y}{(e_{y2} + \sigma_y y_{\text{int}}^{\text{eq}})^2 + \Delta_y^2} g(e_{y2}) \\ 0 \end{bmatrix}, \quad (64)$$

$$\mathbf{H}_3 \triangleq \begin{bmatrix} 0 & 0 \\ -\frac{\Delta_y X_{v_r} (\tilde{u}_r + U_{rd}) \cos(\tilde{\theta} + \theta_d)}{(e_{y2} + \sigma_y y_{\text{int}}^{\text{eq}})^2 + \Delta_y^2} & 1 \end{bmatrix} \begin{bmatrix} \mathbf{h}_y^T \\ \mathbf{h}_{v_r}^T \end{bmatrix}. \quad (65)$$

The function $g(e_{y2})$ is identical to $f(e_y)$ given in (18) and thus the bound (20) applies. The vectors $\mathbf{h}_y(\theta_d, \psi_d, v_r, \chi)$ and $\mathbf{h}_{v_r}(y, y_{\text{int}}, \theta_d, \psi_d, v_r, \chi)$ are given in Appendix C. The system (63)

is a cascaded system, where the UGAS and ULES system (63b) perturbs the dynamics (63a) through \mathbf{H}_3 . The next lemma states the stability properties of (63).

Lemma III.3. *Under the conditions of Theorem III.1, the origin of the system (63) is UGAS and ULES.*

Proof. Consider the nominal system:

$$\begin{bmatrix} \dot{e}_{y1} \\ \dot{e}_{y2} \\ \dot{v}_r \end{bmatrix} = \mathbf{A}_3(e_{y2}) \begin{bmatrix} e_{y1} \\ e_{y2} \\ v_r \end{bmatrix} + \mathbf{B}_3(e_{y2}). \quad (66)$$

The system (66) is similar to the system (22). The only difference is the presence of the unknown constants $\Gamma(s)$ and s . Nevertheless, the bounds $0 < \Gamma_{\inf} < \Gamma(s) \leq \Gamma_{\max}$ from (43-44), $1/\sqrt{s^2+1} < 1$ and $|s|/\sqrt{s^2+1} < 1$ are available. Therefore, applying Lemma II.2 from Appendix B it is possible to conclude UGAS and ULES for the origin of the system (66). Finally, the cascaded system (63) is considered. The perturbing system (63b) is UGAS and ULES, as proved in Lemma III.2. Furthermore the interconnection matrix $\mathbf{H}_3(y, y_{\text{int}}, \theta_d, \psi_d, v_r, \boldsymbol{\chi})$ can be shown to satisfy $\|\mathbf{H}_3\| \leq \delta_3(\|\boldsymbol{\chi}\|)(|y| + |y_{\text{int}}| + |v_r|) + \delta_4(\|\boldsymbol{\chi}\|)$, where $\delta_3(\cdot)$ and $\delta_4(\cdot)$ are some continuous non-negative functions. Therefore, applying [59, Theorem 2] and [60, Lemma 8] it is possible to conclude UGAS and ULES for the cascaded system (63). \square

According to Lemma III.3, under the conditions of Theorem III.1, the origin of the system (63), given by $(e_{y1}, e_{y2}, v_r, \boldsymbol{\chi}) = (0, 0, 0, \mathbf{0})$, is UGAS and ULES. Therefore, the control objectives (30) and (32) are achieved and $\psi_{ss} = -\tan^{-1}(V_y/\sqrt{\Gamma(s)^2 - V_y^2})$.

Remark III.12. Notice that the results in Theorem III.1 also hold for underactuated surface vessels taking the full kinematic and dynamic equations into consideration. In particular, by defining $z = \theta = w_r = q = 0$, the 3D AUV dynamics becomes the 2D USV dynamics given in [39]. The integral LOS guidance law is then given by (35c,35d), and the conditions on its parameters by (39,41). Following the proof of Theorem III.1 for the reduced system, it is seen that the closed-loop system is UGAS and ULES and that the control objectives (30,32,34) are fulfilled with $\psi_{ss} = -\tan^{-1}(V_y/\sqrt{U_{rd}^2 - V_y^2})$.

F. Conclusions

In this section a control strategy for path following of underactuated AUVs in presence of constant irrotational ocean currents acting in any direction of the inertial frame has been developed. It is based on a modified LOS guidance law with integral action in both the vertical and horizontal directions. The three dimensional integral LOS is combined with three feedback controllers in a cascaded configuration and the full kinematic-dynamic closed loop system is analyzed using Lyapunov techniques and nonlinear cascaded systems theory. In particular, the analysis gives explicit conditions on the control design parameters to guarantee UGAS and ULES stability.

IV. SIMULATIONS AND EXPERIMENTS

This last part of the paper presents the results of sea trials where the 2D ILOS guidance law from Section II-B is applied to the CART surface vehicle as well as to the LAUV underwater vehicle. The CART unmanned semi-submersible vehicle (USSV) is a 0.9 [m] long and 0.75 [m] wide robotic platform developed by CNR-ISSIA for emergency towing operations [3]. The light autonomous underwater vehicle (LAUV) has been developed and designed by the Laboratório de Sistemas e Tecnologia Subaquática (LSTS) from the University of Porto in cooperation with OceanScan-MST Lda and is classified as a 'One-man portable AUV' since it can be deployed and controlled by a single operator [55].

The ILOS guidance is implemented in combination with standard proven-in-use PID controllers: the CART vehicle employs a PD heading autopilot and a P thrust controller, while the LAUV is equipped with PID heading, depth and speed controllers. Furthermore, the CART controls its relative velocity via the trust level (RPMs) where for every thrust level a certain relative velocity is obtained [50]. The speed control system of the LAUV automatically combines water speed measurements and absolute speed measurements and chooses the most reliable data [55].

The experimental results are presented in combination with simulation results for a back-to-back comparison, where the simulations are considered as a benchmark for the field tests since they assume ideal conditions and make use of approximated models. Furthermore, the knowledge of the local disturbances is limited. Ideal feedback linearizing controllers such as the ones given in Section III-C are used in the simulations and the gains of the ILOS guidance law from Section II-B (the look ahead distance Δ and the integral gain σ) are chosen according to the bounds (7-8). Some preliminary results of these tests are shown in [50] and [61]. In this paper additional data are presented and a back-to-back comparison between simulations and experimental results is given.

This part of the paper is organized as follows: Sections IV-A and IV-B present the simulations and experiments where the ILOS is applied to the CART USSV. Sections IV-C and IV-D present the simulations and experiments where the ILOS is applied to the LAUV vehicle, and finally Section IV-E gives the conclusions.

A. CART Vehicle, Simulations

The ILOS guidance law (6) in a cascaded configuration with the feedback linearizing surge and yaw controllers (36) and (38) (reduced to 3-DOF, i.e. $w_r = \theta = q = 0$) is applied to the scaled model of a supply ship. The model is scaled to the dimensions of the CART USSV through the *bis* normalization system [10] since no accurate model of the CART vehicle is yet available. The purpose is to analyze the behavior of a vehicle having the same dimensions of the CART in order to tune the gains Δ and σ for the experiments, and to compare the simulation results with the experimental results. Only kinematic current disturbances are considered in the simulations as no information on dynamic disturbances is available from measurements or other data from the field. The supply ship model from [26] is used with the following improved linear damping matrix for maneuvering simulation purposes:

$$\mathbf{D}_{bis} = \begin{bmatrix} 0.076 & 0 & 0 \\ 0 & 0.54 & 0.012 \\ 0 & -0.36 & 0.10 \end{bmatrix}. \quad (67)$$

Notice that $\mathbf{D}_{bis} > 0$ is scaled and is obtained from linearization of more complex nonlinear damping models. The upper bound for the current intensity is selected as $V_{\max} = 0.2$ [m] and the vehicle is required to hold a relative surge velocity $U_{rd} = 0.7$ [m/s]. The chosen values for the guidance law integral gain and look-ahead distance are $\sigma = 0.1$ [m/s] and $\Delta = 5$ [m], and satisfy (7-8) while the desired U_{rd} satisfies Assumption II.5. Notice that the chosen values for Δ , σ and U_{rd} guarantee convergence if dynamic disturbances having maximum intensities of $\kappa_v^{\max} = \kappa_v'^{\max} = 0.035$ [m/s²] are also present in addition to the kinematic current with $V_{\max} = 0.2$ [m]. The gains of the controllers (36) and (38) are set to: $k_{u_r} = 0.5$, $k_{\psi} = 1$, $k_r = 3$. In particular, the values for k_{u_r} , k_{ψ} and k_r are chosen to give a time constant of approximately 1.4 [s] for the \tilde{u}_r first order closed loop system and to make the $\tilde{\psi}$ second order closed loop system overdamped with $\omega_0 = 1$ [rad/s]. The ocean current is set to $V_x = 0.02$ [m/s] and $V_y = -0.05$ [m/s], and equals the drift of the vehicle measured before the test runs.

The simulation procedure resembles the test runs and requires the vehicle to move along two parallel straight lines in order to exhibit the transient response and the steady-state behavior of the ILOS guidance system. The reference paths are two parallel straight lines l_1 and l_2 defined by a point and an angular orientation in the $x - y$ plane:

- l_1 : point (60 [m]; -50 [m]), orientation -130 [deg]
- l_2 : point (70 [m]; -50 [m]), orientation 50 [deg]

At the beginning, the first reference line l_1 is fed to the ILOS. After a while, the vehicles is commanded to turn back and follow the second line l_2 . Figures 3, 4 and 5 show how the vehicle successfully follows the lines l_1 and l_2 , with an average crab angle $\psi_{ss} \approx 4.6$ [deg] for l_1 and $\psi_{ss} \approx -4.6$ [deg] for l_2 , to compensate for the disturbances. It can be seen that choosing the guidance law parameters according to the criteria (7-8) gives smooth convergence.

B. CART Vehicle, Sea Trials

In an extensive set of sea trials the USSV was required to move along the two geo-referenced parallel straight lines l_1 and l_2 to exhibit both the transient response as well as the steady state behavior of the guidance law. The guidance law parameters Δ and σ are set to 5 [m] and 0.1 [m/s], respectively, as suggested by the simulations. The thrust level is set to 20%, which corresponds approximately to 0.7 [m/s] of relative velocity. A simple proportional-derivative control scheme has been implemented to provide the basic auto-heading feature and the gains $k_p = 1$ and $k_d = 0.5$ have been set through field tests to have an overshoot free response. Additional data and results from fine on-the-field tuning of the guidance law parameters Δ and σ can be found in [50].

Figures 6-8 show that the experimental results are in good agreement with the simulations results in Figures 3-5. The CART USSV successfully follows the lines l_1 and l_2 , with an average crab angle $\psi_{ss} \approx 1$ [deg] for l_1 and $\psi_{ss} \approx -5$ [deg] for l_2 , to compensate for the disturbances. The asymmetry in the two crab angles is probably caused by heading dependent disturbances.

C. LAUV Vehicle, Simulations

The ILOS guidance law (6) in a cascaded configuration with the feedback linearizing surge and yaw controllers (36) and (38) (reduced to 3-DOF, i.e. $w_r = \theta = q = 0$) is applied to the mathematical model of the LAUV given in [55] and [62]. In particular, given the low speed motion of the AUV, only linear damping is considered and lift is neglected. Moreover, only kinematic current disturbances are considered in the simulations since underwater motion is analyzed (it is reasonable not to take into account any dynamic disturbances when operating below the wave affected zone in closed loop configuration [10], [47]).

The values for the guidance law look-ahead distance and integral gain are chosen to satisfy (7) and (8), and are $\Delta = 4$ [m] and $\sigma = 0.5$ [m/s]. The desired relative velocity is set to $U_{rd} = 1.2$ [m/s] and fulfills the requirements set by Assumption II.5. The controllers (36) and (38) are implemented with the following gains: $k_{u_r} = 1$, $k_{\psi} = 1$ and $k_r = 2$. The value for k_{u_r} is chosen to give a time constant of 1 [s] for the \tilde{u}_r first order closed loop system. The values chosen for k_{ψ} and k_r make the $\tilde{\psi}$ second order closed loop systems critically damped with $\omega_n = 1$ [rad/s] and $\zeta = 1$. The heading closed loop system is made critically damped to have the fastest possible response without overshoots. A switching system that turns on the horizontal ILOS integrator exclusively when the AUV is located within a certain distance from the desired path is implemented to make the simulations resemble the tests even more. This is done not to have too much integral error and hence to avoid overshoots. The corridor in which the integral action is turned on is 3 [m]

wide and is centered around the desired straight path. Moreover, the LOS used outside this corridor has a horizontal look-ahead distance $\Delta = 5.6$ [m]. A longer Δ is used compared to the in-corridor situation to make the tested ILOS guidance scheme comparable in its gains to other guidance laws that were tested on the same day [61]. It is straightforward to show mathematically through Lemma II.2 that a LOS guidance without integral action in presence of current with $V_{max} = 0.2$ [m/s] and $U_{rd} = 1.2$ [m/s] will make the vehicle enter the corridor.

In order to have simulation results that can be directly compared with the experiments, results from planar way-point following simulations are shown, where a way-point switching system based on the circle of acceptance algorithm is employed [10] and the radius of the way-point acceptance circle is set to 5 [m] as it was done in the experiments. The simulation procedure resembles the test runs and requires the vehicle to move along an 8 shaped path to exhibit the transient response and the steady-state behavior of the ILOS guidance system. An 8 shaped path is used since it contains a complete set of port/starboard maneuvers to test the AUV performance and is defined by 6 way-points. The way-points are located 40 [m] from each other with the longest legs measuring 80 [m] in length. They are placed as shown in Figures 9 and 12. This configuration makes the vehicle hold 4 different courses: -170 [deg], 100 [deg], 10 [deg] and -80 [deg]. The desired depth is set to 3 [m] and the vehicle is initially at rest on the surface with a heading of 180 [deg]. The ocean current is set to $V_x = -0.15$ [m/s] and $V_y = 0.04$ [m/s], and equals the drift of the vehicle measured before the test runs. Figures 9, 10 and 11 show how the vehicle successfully converges to the paths defined by the way-points and crabs to compensate for the disturbances.

D. LAUV Vehicle, Experiments

As explained in Section IV-C, the AUV is required to move along a geo-referenced 8 shaped path identified by 6 way-points to exhibit both the transient response as well as the steady state behavior of the guidance law. The guidance law parameters Δ and σ are set to 4 [m] and 0.5 [m/s], respectively, as suggested by the simulations. The desired absolute/water speed of the vehicle is set to 1.2 [m/s] and the desired depth is set to 3 [m].

Figures 12-14 show that the experimental results are in good agreement with the simulations results given in Figures 9-11. The LAUV successfully follows the lines defined by the way-points and crabbing is achieved to compensate for underwater currents. The crab angles are however often different compared to the simulation results and during the longest 80 [m] long legs the angle varies significantly. This is most probably due to the spatial variation of the current. Nevertheless, the vehicle stays on path as shown in Figure 13. Presumably, the ILOS guidance law (6) adapts the crab angle to compensate the prevailing current and hence it shows robustness with respect to varying currents as well. A more detailed robustness assessment of the ILOS guidance law is given in [41] where process noise and model uncertainty are added via simulations.

E. Conclusion

The ILOS guidance law analyzed and presented in the paper has been successfully applied to the CART and the LAUV vehicles for sea trials to support and validate the theoretical findings.

V. CONCLUSION

This paper has focused on the ILOS guidance solution for path following applications of underactuated marine vehicles in presence of environmental disturbances. First, explicit bounds for the choice of the look-ahead distance and the integral gain of the ILOS guidance

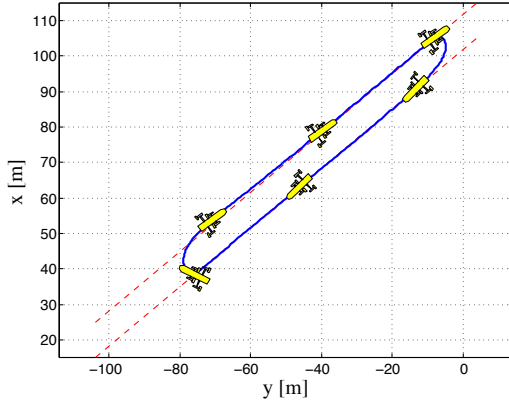


Fig. 3. Simulation of convergence and path following of the CART USSV in presence of constant irrotational ocean currents. The vehicle crabs to compensate for the drift. In this case $\Delta = 5$ [m] and $\sigma = 0.1$ [m/s].

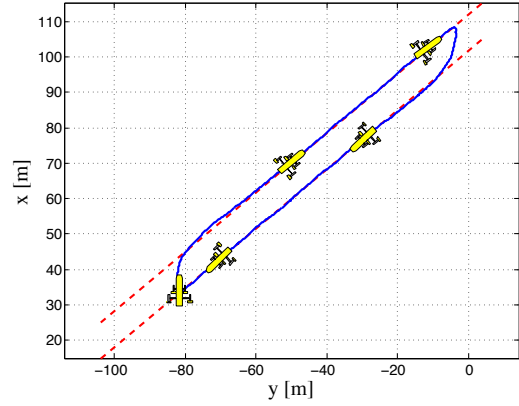


Fig. 6. Experimental ILOS test run of the CART USSV off the coast of Murter, Croatia. Convergence and path following of the USSV is achieved. In this case $\Delta = 5$ [m], $\sigma = 0.1$ [m/s] and the thrust is set to 20%.

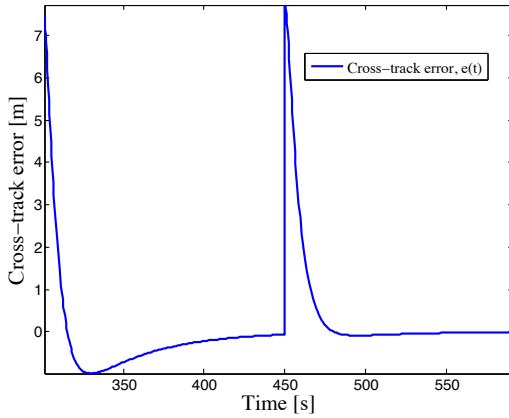


Fig. 4. Cross-track error of the CART USSV from simulations. Notice the overshoot caused by integral action. Afterwards, path following is achieved and the vehicles follows the line l_1 first and the line l_2 afterwards.

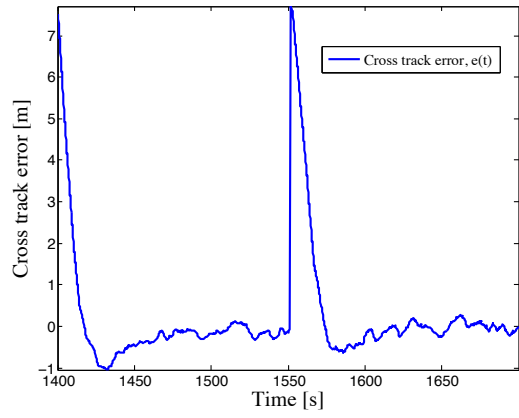


Fig. 7. Cross-track error of the CART USSV from sea trials. Notice the overshoot caused by integral action. Afterwards, path following is achieved for both the l_1 and l_2 lines. Disturbance from waves is present.

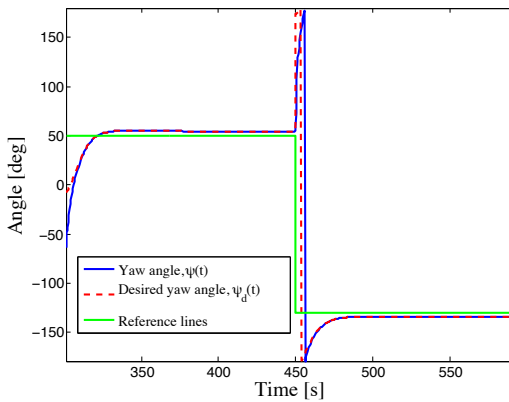


Fig. 5. Yaw angle $\psi(t)$ of the CART USSV from simulations. Notice the steady state crab angle $\psi_{ss} \approx 4.6$ [deg] for the l_1 line and $\psi_{ss} \approx -4.6$ [deg] for the l_2 line.

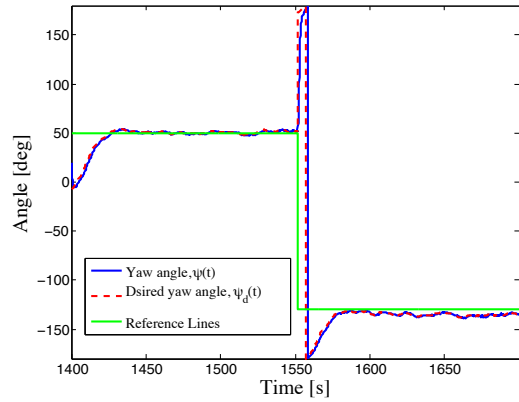


Fig. 8. Yaw angle $\psi(t)$ of the CART USSV from sea trials. Notice that while on path the vehicle holds an average crab angle of $\psi_{ss} \approx 1$ [deg] for the l_1 line and $\psi_{ss} \approx -5$ [deg] for the l_2 line.

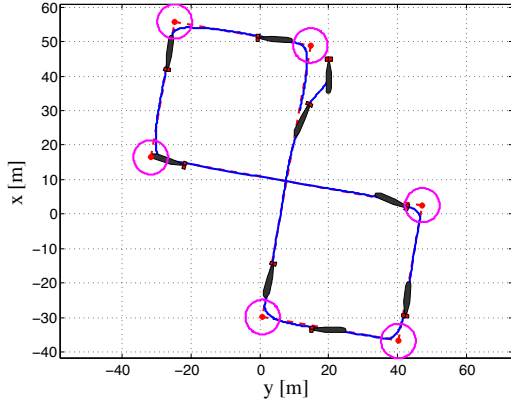


Fig. 9. Simulation of convergence and path following of the LAUV in presence of constant irrotational ocean currents. The vehicle crabs to compensate for the drift. In this case $\Delta_y = 4$ [m] and $\sigma_y = 0.5$ [m/s].

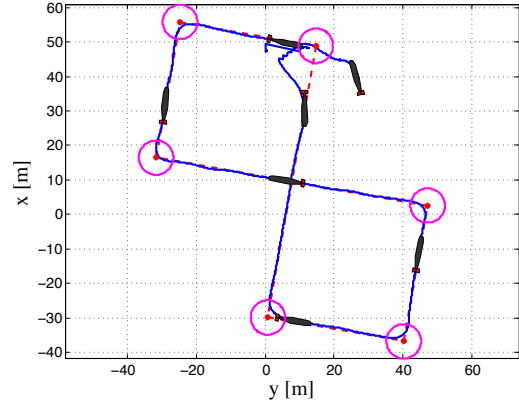


Fig. 12. Experimental ILOS test run of the LAUV in Porto, Portugal. Convergence and path following of the vehicle is achieved. In this case $\Delta_y = 4$ [m], $\sigma_y = 0.5$ [m/s] and the speed is set to 1.2 [m/s].

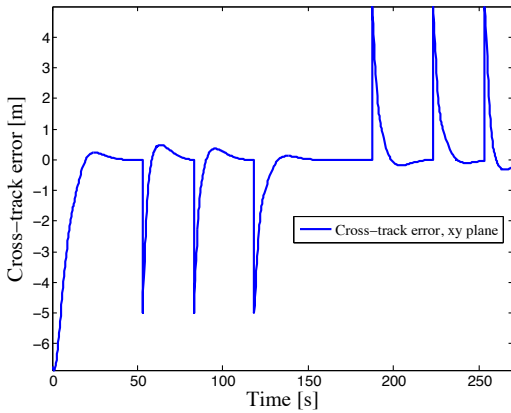


Fig. 10. Cross-track error of the LAUV from simulations. Notice the overshoots caused by the integral action. After the transient, path following is achieved for all the legs defined by the 6 way-points.

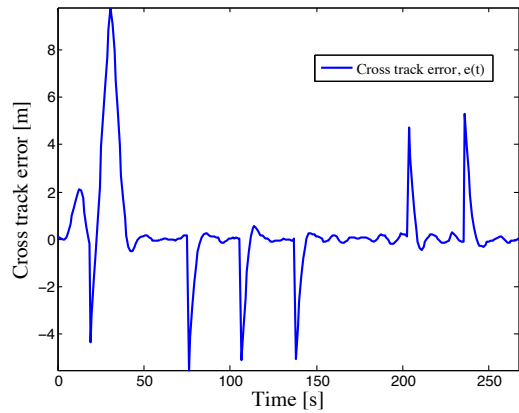


Fig. 13. Cross-track error of the LAUV from sea trials. Notice the overshoots caused by the integral action. After the transient, path following is achieved for all the legs defined by the way-points.

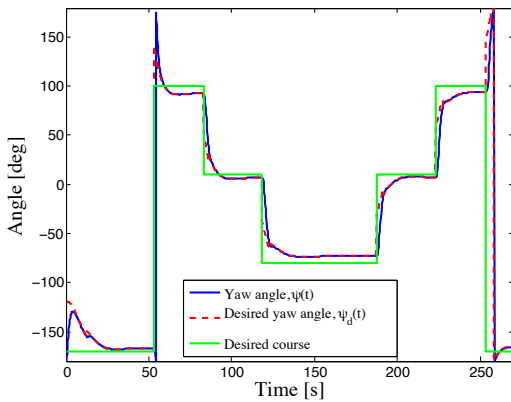


Fig. 11. Yaw angle $\psi(t)$ of the LAUV from simulations. Notice the differences at steady state between the desired course and the heading angle due to crabbing. The vehicle crabs to compensate for the current.

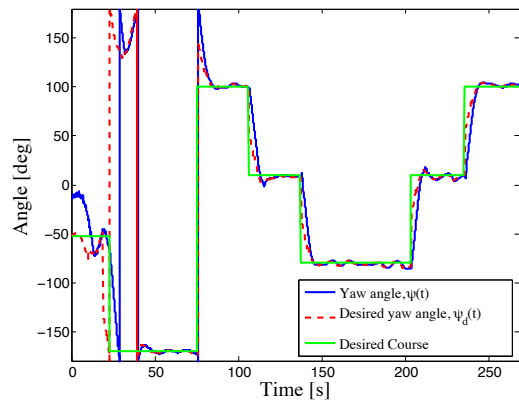


Fig. 14. Yaw angle $\psi(t)$ of the LAUV from sea trials. While on path the vehicle crabs to compensate for the current. The crab angle varies in time since the sea current probably exhibits spatial variations.

have been derived. Disturbances in the form of constant irrotational ocean currents and constant dynamic, attitude dependent, forces have been also taken into account. The stability analysis reveals UGAS and ULES stability properties for the guidance-sway subsystem.

Next, an ILOS control strategy for path following of underactuated AUVs in presence of constant irrotational ocean currents has been developed. The proposed 3D ILOS guidance law embeds integral action in both the vertical and horizontal directions. The full kinematic-dynamic closed loop system is analyzed and the analysis gives explicit conditions on the control design parameters to guarantee UGAS and ULES stability. These results also hold for 2D ILOS guidance of AUVs and USVs by an appurtenant reduction of the system variables.

Finally, the ILOS guidance law has been validated via simulations and experiments. In particular, the ILOS guidance law has been applied to the CART surface vehicle and the LAUV underwater vehicles for sea trials to support the theoretical findings.

APPENDIX A

PROOF OF LEMMA II.1

Equation (12) is written again:

$$s\sqrt{s^2+1} = \frac{V_y}{U_{rd}}s^2 + \frac{\cos(\beta_e)s + \sin(\beta_e)}{U_{rd}|Y^{U_{rd}}|}\kappa_v^{\text{eq}}(s) + \frac{V_y}{U_{rd}}. \quad (68)$$

Notice that $\kappa_v^{\text{eq}}(s)$ is bounded and is defined as the value of $\kappa_v(\gamma_e)$ at equilibrium, i.e. when $\gamma_e = \gamma_e^{\text{eq}} \triangleq -\tan^{-1}(s) - \beta_e - \pi$. This Lemma proves that there exists only one real solution to (68) if Assumptions II.3 and II.5 hold. First, it is shown that there exist real solutions to (68) and then uniqueness is argued. Squaring both sides of (68) gives:

$$p(s) \triangleq (M^2 - U_{rd}^2)s^4 + (2MP_s + N_s^2 - U_{rd}^2)s^2 + 2MN_s s^3 + 2N_s P_s s + P_s^2 = 0, \quad (69)$$

where $M \triangleq V_y$, $N_s \triangleq \kappa_v^{\text{eq}}(s) \cos(\beta_e)/|Y^{U_{rd}}|$ and $P_s \triangleq V_y + \kappa_v^{\text{eq}}(s) \sin(\beta_e)/|Y^{U_{rd}}|$. Hence, $M^2 - U_{rd}^2 < 0$ as long as $U_{rd} > V_{\max}$ which is guaranteed by Assumption II.5. This means that, if Assumption II.5 holds and since N_s and P_s are bounded in s , the function $p(s) \rightarrow -\infty$ as $s \rightarrow \pm\infty$. Furthermore, since $P_s^2 \geq 0, \forall s$, then $p(0) \geq 0$. Therefore, $p(s)$ has at least one real zero, or at least two real zeros, one positive and one negative, if $P_s(s=0) > 0$. This proves the existence of real solutions to (68). The intersections between the curves defined by the two sides of (68) are considered next to show uniqueness:

$$L_1(s^*) \triangleq s^* \sqrt{s^{*2} + 1}, \quad (70)$$

$$L_2(s^*) \triangleq \frac{V_y}{U_{rd}}s^{*2} + \frac{\cos(\beta_e)s^* + \sin(\beta_e)}{U_{rd}|Y^{U_{rd}}|}\kappa_v^{\text{eq}}(s^*) + \frac{V_y}{U_{rd}}. \quad (71)$$

The curve $L_1(s^*)$ is strictly increasing while $L_2(s^*)$ resembles a parabola since $\kappa_v^{\text{eq}}(s^*)$ is bounded as shown in Figure 15. The first derivatives in s^* of $L_1(s^*)$ and $L_2(s^*)$ are analyzed:

$$\frac{dL_1}{ds^*} = \frac{2s^{*2} + 1}{\sqrt{s^{*2} + 1}}, \quad (72)$$

$$\begin{aligned} \frac{dL_2}{ds^*} = & \frac{1}{U_{rd}} \left[2V_y - \frac{d\kappa_v^{\text{eq}}}{d\gamma_e^{\text{eq}}} \cos(\beta_e) \right] s^* \\ & + \frac{\kappa_v^{\text{eq}}(s^*) \cos(\beta_e)}{U_{rd}|Y^{U_{rd}}|} - \frac{d\kappa_v^{\text{eq}}}{d\gamma_e^{\text{eq}}} \frac{\sin(\beta_e)}{U_{rd}|Y^{U_{rd}}|(1+s^{*2})}, \end{aligned} \quad (73)$$

where the property $\frac{d\kappa_v^{\text{eq}}}{ds^*} = \frac{d\kappa_v^{\text{eq}}}{d\gamma_e^{\text{eq}}} \frac{d\gamma_e^{\text{eq}}}{ds^*} = -\frac{d\kappa_v^{\text{eq}}}{d\gamma_e^{\text{eq}}} \frac{1}{1+s^{*2}}$ is used. The following bound holds:

$$\left[\frac{2V_{\max}}{U_{rd}} + \frac{\kappa_v^{\prime \max}}{U_{rd}|Y^{U_{rd}}|} \right] |s^*| + \frac{\kappa_v^{\max} + \kappa_v^{\prime \max}}{U_{rd}|Y^{U_{rd}}|} \geq \frac{dL_2}{ds^*}. \quad (74)$$

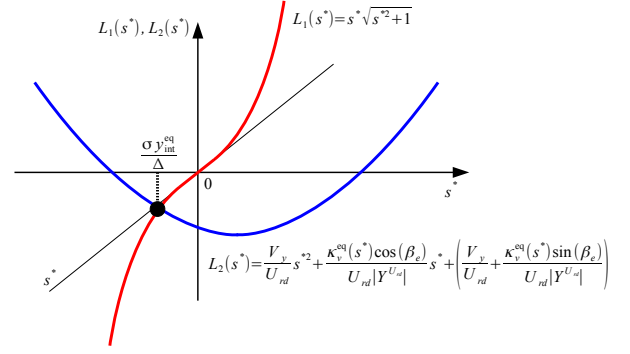


Fig. 15. Graphical solution of (68): $L_1(s^*)$ and $L_2(s^*)$ should intersect exclusively once to make sure that there exists a single equilibrium point. Notice that $L_1(s^*)$ is strictly increasing while $L_2(s^*)$ resembles a parabola since $\kappa_v^{\text{eq}}(s^*)$ is bounded.

Notice that as long as $U_{rd} > 2V_{\max} + (\kappa_v^{\prime \max}/|Y^{U_{rd}}|)$ and $U_{rd} > (2/|Y^{U_{rd}}|)(\kappa_v^{\max} + \kappa_v^{\prime \max})$, which are both guaranteed by Assumption II.5, the following inequality holds for all s^* :

$$\frac{dL_1}{ds^*} > \left[\frac{2V_{\max}}{U_{rd}} + \frac{\kappa_v^{\prime \max}}{U_{rd}|Y^{U_{rd}}|} \right] |s^*| + \frac{\kappa_v^{\max} + \kappa_v^{\prime \max}}{U_{rd}|Y^{U_{rd}}|} \geq \frac{dL_2}{ds^*}. \quad (75)$$

This inequality has two important consequences: if there exist any intersections between L_1 and L_2 , these intersections are transverse intersections. Yet, if there exists an intersection between L_1 and L_2 , then this intersection is unique: since $dL_1/ds^* > dL_2/ds^*$, if the curves intersect in one point, they will never intersect again. The proven existence of real solutions to (68) guarantees that L_1 and L_2 intersect each other and hence it is possible to conclude that the intersection point is unique. To conclude, as long as Assumptions II.3 and II.5 are satisfied, there exists only one real solution s for (68).

APPENDIX B

PROOF OF LEMMA II.2

The system (22) is written again:

$$\begin{bmatrix} \dot{e}_1 \\ \dot{e}_2 \\ \dot{e}_3 \end{bmatrix} = \mathbf{A}_1(e_2) \begin{bmatrix} e_1 \\ e_2 \\ e_3 \end{bmatrix} + \mathbf{B}_1(e_2). \quad (76)$$

Consider the quadratic Lyapunov function candidate:

$$V \triangleq \frac{1}{2}\sigma^2 e_1^2 + \frac{1}{2}e_2^2 + \frac{1}{2}\mu e_3^2, \quad \mu > 0. \quad (77)$$

The time-derivative of V is:

$$\begin{aligned} \dot{V} = & -\frac{\sigma^3 \Delta}{(e_2 + \sigma y_{\text{int}}^{\text{eq}})^2 + \Delta^2} e_1^2 \\ & + \left[\sigma \Delta - U_{rd} \sqrt{(e_2 + \sigma y_{\text{int}}^{\text{eq}})^2 + \Delta^2} \right] \frac{e_2^2}{(e_2 + \sigma y_{\text{int}}^{\text{eq}})^2 + \Delta^2} \\ & + \mu \sin(\psi_{ss} - \beta_e) g(e_2) e_3 + \frac{\Delta}{\sqrt{(e_2 + \sigma y_{\text{int}}^{\text{eq}})^2 + \Delta^2}} e_2 e_3 \\ & + V_y f(e_2) e_2 - \mu \frac{\Delta X^{U_{rd}} V_y}{(e_2 + \sigma y_{\text{int}}^{\text{eq}})^2 + \Delta^2} f(e_2) e_3 \\ & - \mu \left[-Y^{U_{rd}} + \frac{\Delta^2 X^{U_{rd}}}{((e_2 + \sigma y_{\text{int}}^{\text{eq}})^2 + \Delta^2)^{3/2}} \right] e_3^2 \\ & + \mu \left[\frac{U_{rd} \Delta X^{U_{rd}}}{(e_2 + \sigma y_{\text{int}}^{\text{eq}})^2 + \Delta^2} - \frac{\sigma \Delta^2 X^{U_{rd}}}{((e_2 + \sigma y_{\text{int}}^{\text{eq}})^2 + \Delta^2)^{3/2}} \right] \\ & \cdot \frac{e_2 e_3}{\sqrt{(e_2 + \sigma y_{\text{int}}^{\text{eq}})^2 + \Delta^2}} + \frac{\mu \sigma^2 \Delta^2 X^{U_{rd}}}{((e_2 + \sigma y_{\text{int}}^{\text{eq}})^2 + \Delta^2)^2} e_1 e_3 \\ & + \kappa_v(\gamma_e) \cos(\beta_e) \frac{e_2 e_3}{\sqrt{(e_2 + \sigma y_{\text{int}}^{\text{eq}})^2 + \Delta^2}}. \end{aligned} \quad (78)$$

Assumptions II.1-II.5, the inequalities (20-21) and the notation $\bar{e}_1 \triangleq e_1/\sqrt{(e_2 + \sigma y_{\text{int}}^{\text{eq}})^2 + \Delta^2}$, and $\bar{e}_2 \triangleq e_2/\sqrt{(e_2 + \sigma y_{\text{int}}^{\text{eq}})^2 + \Delta^2}$ yield the following bound for \dot{V} :

$$\begin{aligned} \dot{V} &\leq -\Delta(U_{rd} - V_{\max} - \sigma)\bar{e}_2^2 - \mu \left(|Y^{U_{rd}}| - \frac{|X^{U_{rd}}|}{\Delta} \right) e_3^2 \\ &\quad - \sigma^3 \Delta \bar{e}_1^2 + \mu \left[\frac{|X^{U_{rd}}|}{\Delta} (U_{rd} + V_{\max} + \sigma) + 2\kappa_v^{\max} \right] |\bar{e}_2| |e_3| \\ &\quad + \Delta |\bar{e}_2| |e_3| + \frac{\mu \sigma^2 |X^{U_{rd}}|}{\Delta} |\bar{e}_1| |e_3|. \end{aligned} \quad (79)$$

It can be then rearranged as:

$$\dot{V} \leq -W_1(|\bar{e}_1|, |e_3|) - W_2(|\bar{e}_2|, |e_3|), \quad (80)$$

$$\begin{aligned} W_1 &\triangleq \sigma^3 \Delta |\bar{e}_1|^2 - \mu \frac{\sigma^2 |X^{U_{rd}}|}{\Delta} |\bar{e}_1| |e_3| \\ &\quad + \mu \eta \left(|Y^{U_{rd}}| - \frac{|X^{U_{rd}}|}{\Delta} \right) |e_3|^2, \end{aligned} \quad (81)$$

$$W_2 \triangleq \Delta \begin{bmatrix} |\bar{e}_2| & |e_3| \end{bmatrix} \begin{bmatrix} \beta & -\alpha \\ -\alpha & \frac{\alpha(2\alpha-1)}{\beta} \end{bmatrix} \begin{bmatrix} |\bar{e}_2| \\ |e_3| \end{bmatrix}, \quad (82)$$

where $0 < \eta < 1$, $\beta \triangleq U_{rd} - V_{\max} - \sigma$ and α is given by:

$$\alpha \triangleq (1 - \eta) \frac{(U_{rd} - V_{\max} - \sigma)(\Delta |Y^{U_{rd}}| - |X^{U_{rd}}|)}{|X^{U_{rd}}| (U_{rd} + V_{\max} + \sigma) + 2\Delta \kappa_v^{\max}}. \quad (83)$$

The parameter μ is chosen as:

$$\mu \triangleq \frac{\Delta^2 (2\alpha - 1)}{|X^{U_{rd}}| (U_{rd} + V_{\max} + \sigma) + 2\Delta \kappa_v^{\max}}. \quad (84)$$

In (80) the term $\mu(|Y^{U_{rd}}| - |X^{U_{rd}}|/\Delta)|e_3|^2$ has been split in $\eta\mu(|Y^{U_{rd}}| - |X^{U_{rd}}|/\Delta)|e_3|^2$ and $(1 - \eta)\mu(|Y^{U_{rd}}| - |X^{U_{rd}}|/\Delta)|e_3|^2$. This makes it possible to avoid splitting cross terms through Young's inequality as done for instance in [34] and hence shift the analysis on the two quadratic functions W_1 and W_2 . In particular, if both W_1 and W_2 are definite positive then \dot{V} is negative definite. Positive definiteness of W_1 is ensured if (85) and (86) are satisfied:

$$\Delta > \frac{|X^{U_{rd}}|}{|Y^{U_{rd}}|}, \quad (85) \quad \mu < \frac{4\eta\Delta^2 \left[\Delta |Y^{U_{rd}}| - |X^{U_{rd}}| \right]}{\sigma |X^{U_{rd}}|^2}. \quad (86)$$

Notice that condition (85) is met as long as (7) holds. At this point, the choice of η becomes subject to constraints. In particular, it is necessary to show that there exist η such that $0 < \eta < 1$ and that (86) is satisfied. In particular, (86) and (83) lead to the following inequality:

$$\frac{(1 - \eta)(U_{rd} - V_{\max} - \sigma)}{[|X^{U_{rd}}| (U_{rd} + V_{\max} + \sigma) + 2\Delta \kappa_v^{\max}]^2} < \frac{2\eta}{\sigma |X^{U_{rd}}|^2}. \quad (87)$$

It is straightforward to show that $\eta \geq 1/5$ is a sufficient condition for (87) to hold. Hence, if $\eta \geq 1/5$ then μ , defined in (84), satisfies (86). Therefore, without any loss of generality, η is set to $1/5$. Both β and α must fulfill $\beta > 0$ and $\alpha > 1$ to guarantee positive definiteness of W_2 . Assumption II.5 and (8) make sure that $\beta > 0$ while it is easy to check that conditions (7) and (8) imply $\alpha > 1$. Furthermore, $\alpha > 1$ guarantees $\mu > 0$ and ensures positive definiteness of V . Therefore under the conditions stated in Theorem II.1, V , W_1 and W_2 are positive definite and hence, following standard Lyapunov arguments, the system (76) is UGAS. Furthermore, the inequality $W \triangleq W_1 + W_2 \geq \bar{\lambda}_1 |\bar{e}_1|^2 + \bar{\lambda}_2 |\bar{e}_2|^2 + \bar{\lambda}_3 |e_3|^2$ holds in a neighbourhood of the origin for some constants $\bar{\lambda}_1, \bar{\lambda}_2, \bar{\lambda}_3 > 0$ and thus in any ball $\mathcal{B}_r \triangleq \{e_2 | \leq r\}, r > 0$ the function W can be estimated as $W \geq \lambda_1 |e_1|^2 + \lambda_2 |e_2|^2 + \lambda_3 |e_3|^2$ where

$\lambda_i = \bar{\lambda}_i / ((r + \sigma y_{\text{int}}^{\text{eq}})^2 + \Delta^2)$, $i = 1, 2$. This, together with the fact that V is a quadratic function of e_1 , e_2 and e_3 , concludes that (76) is also uniformly locally exponentially stable, ULES.

APPENDIX C

FUNCTIONAL EXPRESSIONS - SECTION III

The expressions F_{u_r} , X_{v_r} , Y_{v_r} , X_{w_r} , Y_{w_r} , Z_{w_r} , F_q and F_r are:

$$F_{u_r}(v_r, w_r, r, q) \triangleq \frac{1}{m_{11}} [(m_{22}v_r + m_{25}r) - (m_{33}w_r + m_{34}q)q], \quad (88)$$

$$X_{v_r}(u_r) \triangleq \frac{m_{25}^2 - m_{11}m_{55}}{m_{22}m_{55} - m_{25}^2} u_r + \frac{d_{55}m_{25} - d_{25}m_{55}}{m_{22}m_{55} - m_{25}^2}, \quad (89)$$

$$Y_{v_r}(u_r) \triangleq \frac{(m_{22} - m_{11})m_{25}}{m_{22}m_{55} - m_{25}^2} u_r - \frac{d_{22}m_{55} - d_{52}m_{25}}{m_{22}m_{55} - m_{25}^2}, \quad (90)$$

$$X_{w_r}(u_r) \triangleq \frac{-m_{34}^2 + m_{11}m_{44}}{m_{33}m_{44} - m_{34}^2} u_r + \frac{d_{44}m_{34} - d_{34}m_{44}}{m_{33}m_{44} - m_{34}^2}, \quad (91)$$

$$Y_{w_r}(u_r) \triangleq \frac{(m_{11} - m_{33})m_{34}}{m_{33}m_{44} - m_{34}^2} u_r - \frac{d_{33}m_{44} - d_{43}m_{34}}{m_{33}m_{44} - m_{34}^2}, \quad (92)$$

$$Z_{w_r} \triangleq \frac{BG_z W m_{34}}{m_{33}m_{44} - m_{34}^2}, \quad (93)$$

$$\begin{aligned} F_r(u_r, v_r, r) &\triangleq \frac{m_{25}d_{22} - m_{22}(d_{52} + (m_{22} - m_{11})u_r)}{m_{22}m_{55} - m_{25}^2} v_r \\ &\quad + \frac{m_{25}(d_{25} + m_{11}u_r) - m_{22}(d_{55} + m_{25}u_r)}{m_{22}m_{55} - m_{25}^2} r, \end{aligned} \quad (94)$$

$$\begin{aligned} F_q(\theta, u_r, w_r, q) &\triangleq -\frac{BG_z W m_{33}}{m_{33}m_{44} - m_{34}^2} \sin(\theta) \\ &\quad + \frac{m_{34}(d_{34} - m_{11}u_r) - m_{33}(d_{44} - m_{34}u_r)}{m_{33}m_{44} - m_{34}^2} q \\ &\quad + \frac{m_{34}d_{33} - m_{33}(d_{43} - (m_{33} - m_{11})u_r)}{m_{33}m_{44} - m_{34}^2} w_r. \end{aligned} \quad (95)$$

The vectors $\mathbf{h}_z \triangleq [h_{z1}, h_{z2}, h_{z3}, h_{z4}, h_{z5}]^T$ and $\mathbf{h}_{w_r} \triangleq [h_{w_r1}, h_{w_r2}, h_{w_r3}, h_{w_r4}, h_{w_r5}]^T$ are defined as:

$$\begin{aligned} h_{z1} &= -\sin(\tilde{\theta} + \theta_d), \quad h_{z3} = h_{z4} = h_{z5} = 0 \\ h_{z2} &= -U_{rd} \left[\frac{\sin(\tilde{\theta})}{\tilde{\theta}} \cos(\theta_d) + \frac{\cos(\tilde{\theta}) - 1}{\tilde{\theta}} \sin(\theta_d) \right] \\ &\quad + w_r \left[\frac{\cos(\tilde{\theta}) - 1}{\tilde{\theta}} \cos(\theta_d) - \frac{\sin(\tilde{\theta})}{\tilde{\theta}} \sin(\theta_d) \right], \\ h_{w_r1} &= \frac{X_{w_r}(\tilde{u}_r + U_{rd}) - X_{w_r}^{U_{rd}}}{\tilde{u}_r} \gamma_{w_r}(z_{\text{int}}, z, w_r) \\ &\quad + w_r \frac{Y_{w_r}(\tilde{u}_r + U_{rd}) - Y_{w_r}^{U_{rd}}}{\tilde{u}_r}, \\ h_{w_r2} &= Z_{w_r} \left[\frac{\sin(\tilde{\theta})}{\tilde{\theta}} \cos(\theta_d) + \frac{\cos(\tilde{\theta}) - 1}{\tilde{\theta}} \sin(\theta_d) \right], \\ h_{w_r3} &= X_{w_r}(\tilde{u}_r + U_{rd}), \quad h_{w_r4} = h_{w_r5} = 0. \end{aligned} \quad (96)$$

Notice that the limits of h_{z2} for $\tilde{\theta} \rightarrow 0$, h_{w_r1} for $\tilde{u}_r \rightarrow 0$ and h_{w_r2} for $\tilde{\theta} \rightarrow 0$ exist and are finite. The vectors $\mathbf{h}_y \triangleq [h_{y1}, h_{y2}, h_{y3}, h_{y4}, h_{y5}, h_{y6}, h_{y7}, h_{y8}]^T$ and $\mathbf{h}_{v_r} \triangleq [h_{v_r1}, h_{v_r2}, h_{v_r3}, h_{v_r4}, h_{v_r5}, h_{v_r6}, h_{v_r7}, h_{v_r8}]^T$ are defined as:

$$\begin{aligned} h_{y2} &= \frac{U_{rd}}{e_{z2}} \left[\frac{\Delta_z}{\sqrt{(e_{z2} + \sigma_z z_{\text{int}}^{\text{eq}})^2 + \Delta_z^2}} - \frac{1}{\sqrt{s^2 + 1}} \right] \\ &\quad - \frac{s}{\sqrt{s^2 + 1}} \frac{Z_{w_r}}{Y_{w_r}^{U_{rd}}} \frac{1}{e_{z2}} \left[\frac{e_{z2} + \sigma_z z_{\text{int}}^{\text{eq}}}{\sqrt{(e_{z2} + \sigma_z z_{\text{int}}^{\text{eq}})^2 + \Delta_z^2}} - \frac{s}{\sqrt{s^2 + 1}} \right], \end{aligned} \quad (98)$$

$$\mathbf{A}_2 \triangleq \begin{bmatrix} -\frac{\sigma_z \Delta_z}{(e_{z2} + \sigma_z z_{\text{int}}^{\text{eq}})^2 + \Delta_z^2} & \frac{\Delta_z}{(e_{z2} + \sigma_z z_{\text{int}}^{\text{eq}})^2 + \Delta_z^2} & 0 \\ -\frac{\sigma_z^2 \Delta_z}{(e_{z2} + \sigma_z z_{\text{int}}^{\text{eq}})^2 + \Delta_z^2} & \left(-\frac{U_{rd}}{\sqrt{(e_{z2} + \sigma_z z_{\text{int}}^{\text{eq}})^2 + \Delta_z^2}} + \frac{\sigma_z \Delta_z}{(e_{z2} + \sigma_z z_{\text{int}}^{\text{eq}})^2 + \Delta_z^2} \right) & \frac{\Delta_z}{\sqrt{(e_{z2} + \sigma_z z_{\text{int}}^{\text{eq}})^2 + \Delta_z^2}} \\ \frac{-\sigma_z^2 \Delta_z^2 X_{w_r}^{U_{rd}}}{((e_{z2} + \sigma_z z_{\text{int}}^{\text{eq}})^2 + \Delta_z^2)^2} & \left(\frac{-U_{rd} \Delta_z X_{w_r}^{U_{rd}}}{((e_{z2} + \sigma_z z_{\text{int}}^{\text{eq}})^2 + \Delta_z^2)^{3/2}} + \frac{\sigma_z \Delta_z^2 X_{w_r}^{U_{rd}}}{((e_{z2} + \sigma_z z_{\text{int}}^{\text{eq}})^2 + \Delta_z^2)^2} + \frac{Z_{w_r}}{\sqrt{(e_{z2} + \sigma_z z_{\text{int}}^{\text{eq}})^2 + \Delta_z^2}} \right) & \left(Y_{w_r}^{U_{rd}} + \frac{\Delta_z^2 X_{w_r}^{U_{rd}}}{((e_{z2} + \sigma_z z_{\text{int}}^{\text{eq}})^2 + \Delta_z^2)^{3/2}} \right) \end{bmatrix}, \quad (99)$$

$$\mathbf{A}_3 \triangleq \begin{bmatrix} -\frac{\sigma_y \Delta_y}{(e_{y2} + \sigma_y y_{\text{int}}^{\text{eq}})^2 + \Delta_y^2} & \frac{\Delta_y}{(e_{y2} + \sigma_y y_{\text{int}}^{\text{eq}})^2 + \Delta_y^2} & 0 \\ -\frac{\sigma_y^2 \Delta_y}{(e_{y2} + \sigma_y y_{\text{int}}^{\text{eq}})^2 + \Delta_y^2} & \left(-\frac{\Gamma(s)}{\sqrt{(e_{y2} + \sigma_y y_{\text{int}}^{\text{eq}})^2 + \Delta_y^2}} + \frac{\sigma_y \Delta_y}{(e_{y2} + \sigma_y y_{\text{int}}^{\text{eq}})^2 + \Delta_y^2} \right) & \frac{\Delta_y}{\sqrt{(e_{y2} + \sigma_y y_{\text{int}}^{\text{eq}})^2 + \Delta_y^2}} \\ \frac{1}{\sqrt{s^2 + 1}} \frac{\sigma_y^2 \Delta_y^2 X_{v_r}^{U_{rd}}}{((e_{y2} + \sigma_y y_{\text{int}}^{\text{eq}})^2 + \Delta_y^2)^2} & \frac{1}{\sqrt{s^2 + 1}} \left(\frac{\Gamma(s) \Delta_y X_{v_r}^{U_{rd}}}{((e_{y2} + \sigma_y y_{\text{int}}^{\text{eq}})^2 + \Delta_y^2)^{3/2}} - \frac{\sigma_y \Delta_y^2 X_{v_r}^{U_{rd}}}{((e_{y2} + \sigma_y y_{\text{int}}^{\text{eq}})^2 + \Delta_y^2)^2} \right) & \left(Y_{v_r}^{U_{rd}} - \frac{\Delta_y^2 X_{v_r}^{U_{rd}}}{\sqrt{s^2 + 1} ((e_{y2} + \sigma_y y_{\text{int}}^{\text{eq}})^2 + \Delta_y^2)^{3/2}} \right) \end{bmatrix}, \quad (100)$$

$$\begin{aligned} h_{y5} &= U_{rd} \sin(\psi_d) \left[\frac{\cos(\tilde{\theta}) - 1}{\tilde{\theta}} \cos(\theta_d) - \frac{\sin(\tilde{\theta})}{\tilde{\theta}} \sin(\theta_d) \right] \\ &\quad - \frac{s \sin(\psi_d)}{\sqrt{s^2 + 1}} \frac{Z_{w_r}}{Y_{w_r}^{U_{rd}}} \left[\frac{\sin(\tilde{\theta})}{\tilde{\theta}} \cos(\theta_d) + \frac{\cos(\tilde{\theta}) - 1}{\tilde{\theta}} \sin(\theta_d) \right], \\ h_{y7} &= \left[U_{rd} \cos(\tilde{\theta} + \theta_d) - \frac{s}{\sqrt{s^2 + 1}} \frac{Z_{w_r}}{Y_{w_r}^{U_{rd}}} \sin(\tilde{\theta} + \theta_d) \right] \\ &\quad \cdot \left[\frac{\sin(\tilde{\psi})}{\tilde{\psi}} \cos(\psi_d) + \frac{\cos(\tilde{\psi}) - 1}{\tilde{\psi}} \sin(\psi_d) \right] \\ &\quad + v_r \left[\frac{\cos(\tilde{\psi}) - 1}{\tilde{\psi}} \cos(\psi_d) - \frac{\sin(\tilde{\psi})}{\tilde{\psi}} \sin(\psi_d) \right], \\ h_{y1} &= h_{y6} = h_{y8} = 0, \quad h_{y3} = \sin(\theta) \sin(\psi), \quad h_{y4} = \cos(\theta) \sin(\psi), \end{aligned} \quad (101)$$

$$\begin{aligned} h_{v_r,2} &= \frac{X_{v_r}^{U_{rd}}}{e_{z2}} \left[\frac{\Delta_z}{\sqrt{(e_{z2} + \sigma_z z_{\text{int}}^{\text{eq}})^2 + \Delta_z^2}} - \frac{1}{\sqrt{s^2 + 1}} \right] \\ &\quad \cdot \gamma_{v_r}(y_{\text{int}}, y, v_r), \\ h_{v_r,4} &= \frac{X_{v_r}(\tilde{u}_r + U_{rd}) - X_{v_r}^{U_{rd}} \cos(\tilde{\theta} + \theta_d)}{\tilde{u}_r} \gamma_{v_r}(y_{\text{int}}, y, v_r) \\ &\quad + v_r \frac{Y_{v_r}(\tilde{u}_r + U_{rd}) - Y_{v_r}^{U_{rd}}}{\tilde{u}_r}, \\ h_{v_r,5} &= \left[\frac{\cos(\tilde{\theta}) - 1}{\tilde{\theta}} \cos(\theta_d) - \frac{\sin(\tilde{\theta})}{\tilde{\theta}} \sin(\theta_d) \right] \\ &\quad \cdot X_{v_r}^{U_{rd}} \gamma_{v_r}(y_{\text{int}}, y, v_r), \\ h_{v_r,8} &= X_{v_r}(\tilde{u}_r + U_{rd}) \cos(\tilde{\theta} + \theta_d), \\ h_{v_r,1} &= h_{v_r,3} = h_{v_r,6} = h_{v_r,7} = 0. \end{aligned} \quad (102)$$

Notice that the limits of h_{y2} for $e_{z2} \rightarrow 0$, h_{y5} for $\tilde{\theta} \rightarrow 0$, h_{y7} for $\tilde{\psi} \rightarrow 0$, $h_{v_r,2}$ for $e_{z2} \rightarrow 0$, $h_{v_r,4}$ for $\tilde{u}_r \rightarrow 0$ and $h_{v_r,5}$ for $\tilde{\theta} \rightarrow 0$ exist and are finite. The expressions $\gamma_{w_r}(z_{\text{int}}, z, w_r)$ and $\gamma_{v_r}(y_{\text{int}}, y, v_r)$ are defined as:

$$\begin{aligned} \gamma_{w_r} &\triangleq -\frac{\Delta_z U_{rd}(z + \sigma_z z_{\text{int}})}{((z + \sigma_z z_{\text{int}})^2 + \Delta_z^2)^{3/2}} + \frac{\Delta_z^2}{((z + \sigma_z z_{\text{int}})^2 + \Delta_z^2)^{3/2}} w_r \\ &\quad + \frac{\sigma_z \Delta_z^2}{((z + \sigma_z z_{\text{int}})^2 + \Delta_z^2)^2} z + \frac{\Delta_z V_z}{(z + \sigma_z z_{\text{int}})^2 + \Delta_z^2}, \end{aligned} \quad (103)$$

$$\begin{aligned} \gamma_{v_r} &\triangleq \frac{\Delta_y \Gamma(s)(y + \sigma_y y_{\text{int}})}{((y + \sigma_y y_{\text{int}})^2 + \Delta_y^2)^{3/2}} - \frac{\Delta_y^2}{((y + \sigma_y y_{\text{int}})^2 + \Delta_y^2)^{3/2}} v_r \\ &\quad - \frac{\sigma_y \Delta_y^2}{((y + \sigma_y y_{\text{int}})^2 + \Delta_y^2)^2} y - \frac{\Delta_y V_y}{(y + \sigma_y y_{\text{int}})^2 + \Delta_y^2}. \end{aligned} \quad (104)$$

REFERENCES

- [1] O. M. Faltinsen, *Sea Loads on Ships and Offshore Structures*. Cambridge University Press, 1990.
- [2] D. Ribas, N. Palomeras, P. Ridaio, M. Carreras, and A. Mallios, "Girona 500 AUV: From survey to intervention," *IEEE/ASME Transactions on Mechatronics*, vol. 17, no. 1, pp. 46–53, 2012.
- [3] G. Bruzzone, M. Bibuli, M. Caccia, and E. Zereik, "Cooperative robotic maneuvers for emergency ship towing operations," in *Proc. of MTS/IEEE Conference OCEANS '13 - Bergen*, 2013, pp. 1–7.
- [4] M. Kurowski and B. Lampe, "AGaPaS: A new approach for search-and-rescue-operations at sea," *Proc. of the Institution of Mechanical Engineers, Part M: Journal of Engineering for the Maritime Environment*, vol. 228, no. 2, pp. 156–165, May 2014.
- [5] T. A. Johansen and T. I. Fossen, "Control allocation - a survey," *Automatica*, vol. 49, no. 5, pp. 1087–1103, 2013.
- [6] E. Y. Hong, T. K. Meng, and M. Chitre, "Online system identification of the dynamics of an autonomous underwater vehicle," in *Proc. of IEEE International Symposium on Underwater Technology*, 2013, pp. 1–10.
- [7] P. Encarnação and A. M. Pascoal, "Combined trajectory tracking and path following: an application to the coordinated control of autonomous marine craft," in *Proc. of the 40th IEEE Conference on Decision and Control*, 2001, pp. 964–969.
- [8] A. P. Aguiar and J. P. Hespanha, "Trajectory-tracking and path-following of underactuated autonomous vehicles with parametric modeling uncertainty," *IEEE Transactions on Automatic Control*, vol. 52, no. 8, pp. 1362–1379, 2007.
- [9] J. E. Da Silva and J. B. Sousa, "A dynamic programming approach for the motion control of autonomous vehicles," in *Proc. of the 49th IEEE Conference on Decision and Control*, 2010, pp. 6660–6665.
- [10] T. I. Fossen, *Handbook of Marine Craft Hydrodynamics and Motion Control*. Hoboken, NJ: John Wiley & Sons, Inc., 2011.
- [11] H. Ashrafioun, K. R. Muske, and L. C. McNinch, "Review of nonlinear tracking and setpoint control approaches for autonomous underactuated marine vehicles," in *Proc. of American Control Conference*, 2010, pp. 5203–5211.
- [12] L. Paull, S. Saeedi, M. Seto, and H. Li, "AUV navigation and localization: A review," *IEEE Journal of Oceanic Engineering*, vol. 39, no. 1, pp. 131–149, 2014.
- [13] P. Encarnação, A. M. Pascoal, and M. Arcak, "Path following for autonomous marine craft," in *Proc. of the 5th IFAC Conference on Manoeuvring and Control of Marine Craft*, 2000, pp. 117–122.
- [14] P. Encarnação and A. M. Pascoal, "3D path following for autonomous underwater vehicle," in *Proc. of the 39th IEEE Conference on Decision and Control*, 2000, pp. 2977–2982.
- [15] L. Lapierre, D. Soetanto, and A. M. Pascoal, "Nonlinear path following with applications to the control of autonomous underwater vehicles," in *Proc. of the 42nd IEEE Conference on Decision and Control*, 2003, pp. 1256–1261.
- [16] K. Y. Pettersen and H. Nijmeijer, "Tracking control of an underactuated surface vessel," in *Proc. of the 37th IEEE Conference on Decision and Control*, 1998, pp. 4561–4566.
- [17] —, "Semi-global practical stabilization and disturbance adaptation for an underactuated ship," in *Proc. of the 39th IEEE Conference on Decision and Control*, 2000, pp. 2144–2149.
- [18] E. Lefeber, K. Y. Pettersen, and H. Nijmeijer, "Tracking control of an underactuated ship," *IEEE Transactions on Control Systems Technology*, vol. 11, no. 1, pp. 52–61, 2003.
- [19] G. Indiveri, M. Aicardi, and G. Casalino, "Robust global stabilization of an underactuated marine vehicle on a linear course by smooth time-

- invariant feedback,” in *Proc. of the 39th IEEE Conference on Decision and Control*, 2000, pp. 2156–2161.
- [20] G. Indiveri and A. A. Zizzari, “Kinematics motion control of an underactuated vehicle: A 3D solution with bounded control effort,” in *Proc. of the 2nd IFAC Workshop on Navigation, Guidance and Control of Underwater Vehicles*, 2008, pp. 73–78.
- [21] K. Do, Z. P. Jiang, and J. Pan, “Underactuated ship global tracking under relaxed conditions,” *IEEE Transactions on Automatic Control*, vol. 47, no. 9, pp. 1529–1536, 2002.
- [22] Z. Li, J. Sun, and S. Oh, “Design, analysis and experimental validation of a robust nonlinear path following controller for marine surface vessels,” *Automatica*, vol. 45, no. 7, pp. 1649–1658, 2009.
- [23] F. A. Papoulias, “Bifurcation analysis of line of sight vehicle guidance using sliding modes,” *International Journal of Bifurcation and Chaos*, vol. 1, no. 4, pp. 849–865, 1991.
- [24] K. Y. Pettersen and E. Lefeber, “Way-point tracking control of ships,” in *Proc. of the 40th IEEE Conference on Decision and Control*, 2001, pp. 940–945.
- [25] T. I. Fossen, M. Breivik, and R. Skjetne, “Line-of-Sight path following of underactuated marine craft,” in *Proc. of the 6th IFAC Conference on Manoeuvring and Control of Marine Craft*, 2003, pp. 244–249.
- [26] E. Fredriksen and K. Y. Pettersen, “Global κ -exponential way-point manoeuvring of ships,” in *Proc. of the 43rd IEEE Conference on Decision and Control*, 2004, pp. 5360–5367.
- [27] R. Skjetne, U. Jørgensen, and A. R. Teel, “Line-of-sight path-following along regularly parametrized curves solved as a generic maneuvering problem,” in *Proc. of the 50th IEEE Conference on Decision and Control*, 2011, pp. 2467–2474.
- [28] M. Breivik and T. Fossen, “Guidance-based path following for autonomous underwater vehicles,” in *Proc. of MTS/IEEE Conference OCEANS ’05*, 2005, pp. 2807–2814.
- [29] M. Breivik and T. I. Fossen, “Principles of guidance-based path following in 2D and 3D,” in *Proc. of the 44th IEEE Conference on Decision and Control*, 2005, pp. 627 – 634.
- [30] E. Fredriksen and K. Y. Pettersen, “Global κ -exponential way-point maneuvering of ships: theory and experiments,” *Automatica*, vol. 42, no. 4, pp. 677–687, 2006.
- [31] E. Børhaug, A. Pavlov, and K. Y. Pettersen, “Straight line path following for formations of underactuated underwater vehicles,” in *Proc. of the 46th IEEE Conference on Decision and Control*, 2007, pp. 2905–2912.
- [32] A. P. Aguiar and A. M. Pascoal, “Modeling and control of an autonomous underwater shuttle for the transport of benthic laboratories,” in *Proc. of MTS/IEEE Conference OCEANS ’97*, 1997, pp. 888–895.
- [33] V. Bakarić, Z. Vukić, and R. Antonić, “Improved basic planar algorithm of vehicle guidance through waypoints by the line of sight,” in *Proc. of the First International Symposium on Control, Communications and Signal Processing*, 2004, pp. 541–544.
- [34] E. Børhaug, A. Pavlov, and K. Y. Pettersen, “Integral LOS control for path following of underactuated marine surface vessels in the presence of constant ocean currents,” in *Proc. of the 47th IEEE Conference on Decision and Control*, 2008, pp. 4984–4991.
- [35] M. Breivik and T. I. Fossen, “Guidance laws for planar motion control,” in *Proc. of the 47th IEEE Conference on Decision and Control*, 2008, pp. 570–577.
- [36] A. M. Lekkas and T. I. Fossen, “Integral los path following for curved paths based on a monotone cubic hermite spline parametrization,” *IEEE Transactions on Control Systems Technology*, vol. 22, no. 6, pp. 2287–2301, Nov 2014.
- [37] T. I. Fossen, K. Y. Pettersen, and R. Galeazzi, “Line-of-sight path following for dubins paths with adaptive sideslip compensation of drift forces,” *IEEE Transactions on Control Systems Technology*, vol. 23, no. 2, pp. 820–827, March 2015.
- [38] T. I. Fossen and K. Y. Pettersen, “On uniform semiglobal exponential stability (usges) of proportional line-of-sight guidance laws,” *Automatica*, vol. 50, no. 11, pp. 2912–2917, Nov 2014.
- [39] W. Caharija, M. Candeloro, K. Y. Pettersen, and A. J. Sørensen, “Relative velocity control and integral LOS for path following of underactuated surface vessels,” in *Proc. of the 9th IFAC Conference on Manoeuvring and Control of Marine Craft*, 2012, pp. 380–385.
- [40] W. Caharija, K. Y. Pettersen, J. T. Gravdahl, and E. Børhaug, “Path following of underactuated autonomous underwater vehicles in the presence of ocean currents,” in *Proc. of the 51st IEEE Conference on Decision and Control*, 2012, pp. 528–535.
- [41] W. Caharija, K. Y. Pettersen, A. J. Sørensen, M. Candeloro, and J. T. Gravdahl, “Relative velocity control and integral LOS for path following of ASVs: Merging intuition with theory,” *Proc. of the Institution of Mechanical Engineers, Part M: Journal of Engineering for the Maritime Environment*, vol. 228, no. 2, pp. 180–191, 2014.
- [42] W. Caharija, K. Y. Pettersen, and J. T. Gravdahl, “Path following of underactuated surface vessels in presence of unknown constant environmental forces: Preliminary results,” in *Proc. of the 9th IFAC Conference on Control Applications in Marine Systems*, 2013, pp. 85–90.
- [43] T. Kinoshita and F. Imado, “The application of an UAV flight simulator - the development of a new point mass model for an aircraft,” in *Proc. of the SICE-ICASE International Joint Conference*, Oct 2006, pp. 4378–4383.
- [44] W. Caharija, K. Y. Pettersen, J. T. Gravdahl, and A. J. Sørensen, “Topics on current compensation for path following applications of underactuated underwater vehicles,” in *Proc. of the 3rd IFAC Workshop on Navigation, Guidance and Control of Underwater Vehicles*, 2013, pp. 184–191.
- [45] R. M. Isherwood, “Wind resistance of merchant ships,” *Transcripts of the Royal Institution of Naval Architects*, vol. 115, pp. 327–338, 1972.
- [46] W. Blendermann, “Parameter identification of wind loads on ships,” *Journal of Wind Engineering and Industrial Aerodynamics*, vol. 51, no. 3, pp. 339–351, 1994.
- [47] S. Fan and C. A. Woolsey, “Underwater vehicle control and estimation in nonuniform currents,” in *Proc. of American Control Conference*, 2013, pp. 1400–1405.
- [48] O. J. Sjørdalen and O. Egeland, “Exponential stabilization of non-holonomic chained systems,” *IEEE Transactions on Automatic Control*, vol. 40, no. 1, pp. 35–49, 1995.
- [49] OCIMF, *Prediction of Wind and Current Loads on VLCCs*. London, UK: Oil Companies International Marine Forum, 1977.
- [50] M. Bibuli, W. Caharija, K. Y. Pettersen, G. Bruzzone, M. Caccia, and E. Zereik, “ILOS guidance - experiments and tuning,” in *Proc. of the 19th IFAC World Congress*, 2014, pp. 4209–4214.
- [51] W. Caharija, K. Y. Pettersen, and J. T. Gravdahl, “Path following of marine surface vessels with saturated transverse actuators,” in *Proc. of American Control Conference*, 2013, pp. 546–553.
- [52] M. S. Wiig, T. R. Krogstad, and K. Y. Pettersen, “Uniform semiglobal exponential stability of integral Line-of-Sight guidance laws,” in *Proc. of the 10th IFAC Conference on Manoeuvring and Control of Marine Craft*, 2015, pp. 61–68.
- [53] H. Khalil, *Nonlinear Systems*, 3rd ed. Upper Saddle River, NJ, USA: Pearson Education International inc., 2000.
- [54] Ø. Hegrenæs, “Autonomous navigation for underwater vehicles,” Ph.D. dissertation, NTNU, Trondheim, Norway, 2010, NTNU thesis 2010: 101.
- [55] J. E. Da Silva, B. Terra, R. Martins, and J. B. Sousa, “Modeling and simulation of the LAUV autonomous underwater vehicle,” in *Proc. of the 13th IEEE IFAC International Conference on Methods and Models in Automation and Robotics*, 2007.
- [56] M. Krstic, “Input delay compensation for forward complete and strict-feedforward nonlinear systems,” *IEEE Transactions on Automatic Control*, vol. 55, no. 2, pp. 287–303, Feb 2010.
- [57] W. Caharija, K. Y. Pettersen, J. T. Gravdahl, and E. Børhaug, “Integral LOS guidance for horizontal path following of underactuated autonomous underwater vehicles in the presence of vertical ocean currents,” in *Proc. of American Control Conference*, 2012, pp. 5427–5434.
- [58] M. Morgado, P. Batista, P. Oliveira, and C. Silvestre, “Position USBL/DVL sensor-based navigation filter in the presence of unknown ocean currents,” *Automatica*, vol. 47, no. 12, pp. 2604–2614, 2011.
- [59] E. Panteley and A. Loria, “On global uniform asymptotic stability of nonlinear time-varying systems in cascade,” *Systems and Control Letters*, vol. 33, no. 2, pp. 131–138, 1998.
- [60] E. Panteley, E. Lefeber, A. Loria, and H. Nijmeijer, “Exponential tracking control of a mobile car using a cascaded approach,” in *Proc. of IFAC Workshop on Motion Control*, 1998, pp. 221–226.
- [61] W. Caharija, K. Y. Pettersen, P. Calado, and J. Braga, “A comparison between the ilos guidance and the vector field guidance,” in *Proc. of the 10th IFAC Conference on Manoeuvring and Control of Marine Craft*, 2015, pp. 89–94.
- [62] Laboratório de Sistemas e Tecnologia Subaquática (LSTS), “DUNE: Unified navigation environment,” <http://lsts.fe.up.pt/software/dune>, April 2014, university of Porto.